AN ANALYTICAL AND EXPERIMENTAL INVESTIGATION OF THE PERFORMANCE OF A DIRECT ACTING THRUST AUGMENTER UTILIZING A ROTATING DISK TO INDUCE UNSTEADY FLOW

A THESIS

Presented to the

Faculty of the Graduate Division

by

Carl Herbert McNair, Jr.

In Partial Fulfillment

of the Requirements for the Degree

Master of Science in Aerospace Engineering

Georgia Institute of Technology

June, 1963

In presenting the dissertation as a partial fulfillment of the requirements for an advanced degree from the Georgia Institute of Technology, I agree that the Library of the Institution shall make it available for inspection and circulation in accordance with its regulations governing materials of this type. I agree that permission to copy from, or to publish from, this dissertation may be granted by the professor under whose direction it was written, or, in his absence, by the dean of the Graduate Division when such copying or publication is solely for scholarly purposes and does not involve potential financial gain. It is understood that any copying from, or publication of, this dissertation which involves potential financial gain will not be allowed without written permission.

6D
12T

AN ANALYTICAL AND EXPERIMENTAL INVESTIGATION OF THE PERFORMANCE OF A DIRECT ACTING THRUST AUGMENTER UTILIZING A ROTATING DISK TO INDUCE UNSTEADY FLOW

Approved:

James E. Hubbartt

Robin B. Gray

Thomas W. Jackson

Date Approved by Chairman: May 27, 1963

ACKNOWLEDGMENTS

The author wishes to express his sincere appreciation to Professor James E. Hubbartt for the valuable guidance and encouragement he extended throughout all phases of this investigation.

A debt of gratitude is acknowledged to Dr. Robin B. Gray and Dr. Thomas W. Jackson for their review and comments on the material contained herein.

Further thanks go to Mr. George W. Cook for his assistance in the construction of the experimental apparatus and to Lockheed-Georgia Company for the use of their test model.

TABLE OF CONTENTS

LIST OF ILLUSTRATIONS

LIST OF ILLUSTRATIONS (Continued)

LIST OF SYMBOLS

A	Non-dimensional speed of sound ratio, a/a_o
a	Speed of sound, feet per second
c	Flow Coefficient
L	Arbitrary duct length
M	Momentum
m	Mass flow per unit of cross sectional area
O	Terms of order and above
P	Riemann variable, $\frac{2}{\gamma-1}$ A + U
p	Pressure
psi	Pounds per square inch
Q	Riemann variable, $\frac{2}{\gamma-1}$ A - U
R	Gas constant
RPM	Revolutions per minute
S	Non-dimensional entropy, $\frac{s}{\gamma R}$
s	Entropy
T	Temperature
t	Time
U	Non-dimensional velocity ratio, u/a_o
u	Flow velocity, feet per second
w	Weight flow of air, pounds per second
x	Distance measured parallel to duct axis
Z	Any Flow Property

α Cross sectional area

β Wave reflection time, inlet to exit and return

γ Ratio of specific heats

Δ Incremental change in value

η Augmentation efficiency factor

λ Thrust Augmentation, $\frac{M_T}{M_{ss}}$

ρ Density of air

τ Non-dimensional time

SUBSCRIPTS

a Ambient

d Disk

e Exit

f End of period

i Inlet

o Initial conditions at reference state

p Primary flow

ss Steady state

s Secondary flow

T Total

us Unsteady flow

1 Period one

2 Period two

SUPERSCRIPT

o Total or stagnation value

SUMMARY

The purpose of this study is to investigate the performance of an unsteady flow augmentation system both analytically and experimentally.

A solution for the augmentation effects due to unsteady flow in a constant area duct is obtained using a numerical-graphical integration procedure. This solution provides a basis for determining the accuracy of the derived analytical expression for the same flow problem.

By limiting the development of the unsteady flow wave equations to a first order analysis, it is possible to derive in closed form an approximate analytical expression for the augmentation ratio and mass flow ratio due to unsteady flow in both a constant area and a diverging duct. The comparison of the analytical solution to the numerical solution for a constant area duct is within ten per cent for flow pressure ratios up to 1.945 thus giving confidence in the simpler approximate theory.

For fixed periods of unsteady flow, the augmentation ratio increases as the pressure of the high pressure primary flow decreases. Increasing the period of inlet exposure to ambient air and decreasing the period of exposure to the high pressure flow also increases the augmentation.

An experimental investigation was conducted to verify the performance predicted by the theoretical analysis. Unsteady flow in a

constant area duct was induced using a slotted rotating disk in a region of high pressure flow. Tests were conducted varying the duct length, inlet position, speed of rotation and the pressure ratio.

Performance of the test apparatus was not as high as that predicted by the theory, however it was shown experimentally that:

(1) The induced unsteady flow does improve the performance of the test apparatus as compared to its performance under steady flow conditions.

(2) Performance improves as the pressure ratio is decreased.

(3) Rotation speeds for which the best performance is obtained are in the same range as those determined from the theory.

Some factors which affect the performance of the system were either uncontrolled or not considered during this exploratory investigation. It is recommended that further investigation of performance of this type thrust augmenter include modifications of the design to include the shape and size of the disk slots, inlet configuration, and duct divergence. If subsequent investigations include these design factors, it is felt that the test apparatus performance can be brought into closer agreement with the theory.

CHAPTER I

INTRODUCTION

A continuing demand for higher performance of jet propulsion systems is making it increasingly necessary for the engineer to develop thrust augmentation devices which will improve performance without sacrificing efficiency or power to weight ratios. Present methods of augmentation are mostly of the direct acting steady-flow viscous type which provide a marginal increase in performance while accepting increases in weight and physical dimensions. Therefore, it becomes desirable to investigate new means of energy transfer which will provide the desired augmentation while avoiding some of the disadvantages associated with present day systems.

Since the principles of steady flow type devices have been advanced to their reasonable limit, it is apparent that the propulsion engineer must look to unsteady flow for a solution to the problem. Foa[1*] has proposed using unsteady flow which when adjusted to the frame of reference of the flow field becomes steady in that frame. This in turn he calls "crypto steady flow." An adaptation of this crypto steady flow analysis to an augmentation device will provide the direct transfer of energy from one steady flow to another by means of moving pressure fields. This transfer of mechanical energy by the pressure waves allows for a higher efficiency than could be attained by direct transfer of

---

*Superscript numbers refer to items in the Bibliography.

energy in a steady flow mixing system.

Several aircraft companies are presently working on systems to provide thrust augmentation. Hiller Aircraft[2] has had considerable success in the development of a pure unsteady flow device utilizing a pulse reactor to generate the unsteady flow field. Lockheed Aircraft[3] employs a functional augmentation system utilizing multiple ejectors operating under steady flow principles. McDonnell Aircraft[4] has conducted experimental tests with a new type augmenter based on the crypto steady principle conceived by Foa.[5] Early tests indicate that this principle is applicable to an engine system and will produce augmentation in accordance with the theory.

The purpose of this study is to investigate still another manner in which to achieve thrust augmentation. An unsteady flow field will be generated by rotating a slotted disk in a region of steady flow. The induced unsteady flow will then be directed through an augmenting duct. The theoretical analysis will utilize the unsteady flow wave equations for investigating the characteristics and potential of this type of augmentation system. The exit conditions of the flow will be related to the inlet conditions by examining the action of the expansion and compression waves within the duct.

An analytical expression will be developed to determine the actual augmentation to be expected under varying inlet conditions. Due to the complexity of the wave equations and the nature of the flow, it will be necessary to limit the development to a first order analysis. The cases of a constant area and a diverging duct will be developed similarly and their results subjected to a comparative analysis.

As in any engineering development, the theory should be substantiated by experimental data before it can be deemed acceptable. Therefore, the analytical results will be applied to an experimental test apparatus to examine the validity of the development. It is realized that the design of a functional device is dependent upon many variable parameters some of which cannot be incorporated into a theoretical analysis, hence an extensive design program would be necessary to achieve optimum results. Time limitations for the present study allow only for exploratory experimental investigations.

CHAPTER II

THE PHYSICAL PROBLEM AND THE GENERAL UNSTEADY FLOW EQUATIONS

In its most simple representation, the problem reduces to one of injecting a slug of air into a rigid duct in which the flow parameters change with distance, x, and time, t. In order to determine the flow properties at any station within the duct, it is necessary to develop the equations of motion for one-dimensional unsteady flow. The general solution of the one-dimensional unsteady flow equation as briefly outlined below can be found in more detail in any standard text on unsteady flow.[1,6,7]

As stated by Foa,[1] all flow properties for any given area, position, and time are specified by three independent state parameters. For this study, the parameters selected are: a (speed of sound), s (specific entropy), and u (flow velocity relative to the duct frame of reference).

The relationship of these parameters to each other must be developed from the equations of continuity, motion and energy (neglecting friction and body forces).

$$\frac{1}{\rho}\frac{\partial \rho}{\partial t} + \frac{u}{\rho}\frac{\partial \rho}{\partial x} + \frac{\partial u}{\partial x} + \frac{u}{\alpha}\frac{\partial \alpha}{\partial x} = 0 \qquad (1)$$

$$\frac{\partial u}{\partial t} + u\frac{\partial u}{\partial x} = -\frac{a^2}{\gamma p} \qquad (2)$$

$$d \ln \rho = \frac{2}{\gamma - 1}\frac{da}{a} - \frac{ds}{R} \qquad (3)$$

$$d \ln p = \frac{2\gamma}{\gamma-1} \frac{da}{a} - \frac{ds}{R} \tag{4}$$

Eliminating ρ between Equations (1) and (3) and eliminating p between Equations (2) and (4) then adding and subtracting these results gives:

$$\frac{\partial}{\partial t}\left(\frac{2}{\gamma-1} a \pm u\right) + (u \pm a) \frac{\partial}{\partial x}\left(\frac{2}{\gamma-1} a \pm u\right) = -au \frac{d \ln \alpha}{dx} + \frac{a}{R}\left(\frac{Ds}{Dt} \pm \frac{a}{\gamma} \frac{\partial s}{\partial x}\right) \tag{5}$$

This is a non-linear partial differential equation the left side of which represents the total time derivatives of the functions $\frac{2}{\gamma-1} a \pm u$ in the directions $\frac{dx}{dt} = u \pm a$. Hence the equations can be numerically integrated along the lines with slopes $\frac{dx}{dt} = u \pm a$. These lines and the particle path lines $\frac{dx}{dt} = u$ are the characteristics of Equations (5).

The slopes $\frac{dx}{dt} = u \pm a$ represent the speeds of propagation of small disturbances relative to the duct walls. Since the flow in the duct is concerned with changes from ambient conditions of the initial state, the zero of entropy will be established at this reference state, hereafter designated by subscript "o". Thus the following non-dimensionalized terms can now be used in equations (5).

$$A = \frac{a}{a_o} \qquad P = \frac{2}{\gamma-1} A + U$$

$$U = \frac{u}{u_o} \qquad Q = \frac{2}{\gamma-1} A - U \tag{6}$$

$$S = \frac{s}{\gamma R}$$

If $\frac{\delta_{\pm}}{\delta t}\left(\frac{2}{\gamma-1}a \pm u\right)$ represents $\frac{\partial}{\partial t} + (u \pm a)\frac{\partial}{\partial x}$, the differentiation with respect to time along the characteristic, Equations (5) become

$$\frac{1}{a_o}\frac{\delta_+ P}{\delta t} = -AU\frac{d\ln\alpha}{dx} + \frac{1}{a_o}A\frac{\delta_+ S}{\delta t} + (\gamma-1)\frac{A}{a_o}\frac{DS}{Dt} \tag{7}$$

$$\frac{1}{a_o}\frac{\delta_- Q}{\delta t} = -AU\frac{d\ln\alpha}{dx} + \frac{A}{a_o}\frac{\delta_- S}{\delta t} + (\gamma-1)\frac{A}{a_o}\frac{DS}{Dt} \tag{8}$$

Equation (7) gives the rate of change of the variable P along the P characteristic $\frac{dx}{dt} = U + A$ and Equation (8) gives the rate of change of the variable Q along the Q characteristic $\frac{dx}{dt} = U - A$. If P and Q are known at any point, then A, U and the slopes of the characteristics can be determined at that point. From Equations (6), the following relations for A and U are derived in terms of P and Q.

$$U = \frac{P - Q}{2} \qquad A = \frac{\gamma - 1}{4}(P + Q) \tag{9}$$

The variables P and Q are sometimes called the "Riemann Variables" and throughout this development, the flow properties will be expressed in terms of these variables.

For the problem under study, the duct is open at both ends and the flow equations must be developed by examining the wave propagation from the inlet to the exit and its continued reflection therefrom. As stated by Foa,[1] the three dimensional wave phenomena through which a flow senses the external conditions and adapts itself to them at the open end are too complex for analysis. Therefore it is assumed that the sensing and adaptation takes place instantaneously. This assumption is

easily justified since the time required for a wave to travel across the open end section is quite small compared to the time required for any significant change to take place in the flow parameters.

Since the flow is subsonic at the exit in the case being studied, the boundary condition to be applied at the exit is that the exit pressure must equal the ambient pressure. It is physically apparent therefore that if a pressure wave propagates downstream to the exit, an expansion wave must be reflected from the exit to maintain the exit pressure.

With subscript e denoting exit conditions, Equations (9) become:

$$U_e = \frac{P_e - Q_e}{2} \qquad A_e = \frac{\gamma - 1}{4}(P_e + Q_e) \tag{10}$$

From the Second Law of Thermodynamics,

$$s_e - s_o = c_p \ln A_e - R \ln \frac{p_e}{p_o} \tag{11}$$

In this case, the ground state s_o is designated as zero and in non-dimensional form, Equation (11) becomes

$$S_e = \frac{2}{\gamma - 1} \ln A_e - \frac{1}{\gamma} \ln \frac{p_e}{p_o} \tag{12}$$

Rearrangement gives

$$A_e = \left(\frac{p_e}{p_o}\right)^{\frac{\gamma-1}{2\gamma}} e^{\left(\frac{\gamma-1}{2}\right)S_e} \tag{13}$$

Since the imposed boundary conditions prescribe that the pressure at the exit be ambient pressure and if $S_e = S_o = 0$, $A_e = 1$ from Equation (13). Applying this result to Equation (10), it is then obvious that $P_e + Q_e$ is a constant, so that any increase in P must be in conjunction with an associated decrease in Q of the same value. Since a compression wave P is reflected from the exit as an expansion wave Q, the relationship between the two at the exit is established as $\Delta P_e = - \Delta Q_e$.

The unsteady flow of the slug of air at the duct inlet will be treated as a quasi-steady flow because $\frac{\partial z}{\partial t} << u \frac{\partial z}{\partial x}$ where z represents any flow property. That is to say that the convective time rate of change greatly exceeds the non-stationary term. Thus, the non-stationary term can be dropped reducing the solution at any instant of time to the steady flow solution. This is defined as "quasi-steady" flow.

For a quasi-steady flow at the inlet, the energy equation from the First Law of Thermodynamics can be written as

$$A_i^2 + \frac{\gamma-1}{2} v_i^2 = A_i^{o2} \tag{14}$$

where A_i^o represents the nondimensional speed of sound at the stagnation temperature T_i^o. A_i^o can also be expressed in terms of the change in value of the speed of sound from ambient conditions.

$$\frac{a_i^o}{a_o} - \frac{a}{a_o} = \frac{\Delta a_i}{a_o} \tag{15}$$

$$A_i^o = 1 + \frac{\Delta a_i^o}{a_o} \tag{16}$$

Applying the relationships of Equations (9), Equation (14) can be written

$$\frac{\gamma+1}{4}\left(P_i^2 + Q_i^2\right) - \frac{3-\gamma}{2} P_i Q_i = \frac{4}{\gamma-1} A_i^{o^2} \tag{17}$$

This completes the development of the unsteady inflow as a quasi-steady process. From this point, efforts will be directed towards obtaining an expression relating the wave action within the duct in a closed form solution.

Equation (17) must be rearranged so that it is in terms of ΔP_i and ΔQ_i and can be related to the known boundary condition $\Delta P_e = -\Delta Q_e$. From Equations (9),

$$P_i = \frac{2}{\gamma - 1} A_i + U_i \qquad Q_i = \frac{2}{\gamma - 1} A_i - U_i \tag{18}$$

It is convenient to reference P_i and Q_i from values P_o and Q_o corresponding to the undisturbed conditions $u = 0$ and $a = a_o$. At which conditions, $U_i = 0$, $A_i = 1$, thus Equation (18) becomes

$$P_{o_i} = Q_{o_i} = \frac{2}{\gamma - 1} \tag{19}$$

$$\Delta P_i = P_i - P_{o_i} = P_i - \frac{2}{\gamma - 1} \tag{20}$$

$$P_i = \Delta P_i + \frac{2}{\gamma - 1} \qquad Q_i = \Delta Q_i + \frac{2}{\gamma - 1} \tag{21}$$

Substituting these relations into Equation (17) and solving for ΔP_i in terms of ΔQ_i and A_i^o yields

$$\left(\frac{\gamma+1}{2}\right)\Delta P_i = -\left(2 - \frac{2-\gamma}{2}\Delta Q_i\right) + \left\{\left(2 - \frac{2-\gamma}{2}\Delta Q_i\right)^2 - (\gamma+1)\left[\frac{\gamma+1}{4}\Delta Q_i^2 + 2\Delta Q_i + \frac{4}{\gamma-1} - \frac{4}{\gamma-1}\left(A_i^o\right)^2\right]\right\}^{\frac{1}{2}} \quad (22)$$

The complexity of this equation makes it extremely difficult to handle when solving for ΔP_i in a closed form solution. However, the expression can be simplified by expanding in a Taylor's series. To second order in $\frac{a_i^o}{a}$ and ΔQ_i, the resulting expression is

$$\Delta P_i = -\Delta Q_i + \frac{4}{\gamma-1}\frac{\Delta a_i^o}{a_o} - \Delta Q_i^2 + \frac{4}{\gamma-1}\frac{\Delta a_i^o}{a_o}\Delta Q_i - \frac{4}{(\gamma-1)^2}\left(\frac{\Delta a_i^o}{a_o}\right)^2 + O\left[(\Delta Q_i)^3, \frac{\Delta a_i^o}{a_o}(\Delta Q_i)^2, \left(\frac{\Delta a_i^o}{a_o}\right)^2 \Delta Q_i, \left(\frac{\Delta a_i^o}{a_o}\right)^3\right] \quad (23)$$

This expression will be utilized in the subsequent closed form analysis.

Through Equation (22), all flow properties at the inlet station are established and can be further related through the exit condition $\Delta P_e = -\Delta Q_e$ which was determined earlier. By examining the values of the characteristics at the exit, the velocity and mass flow can be obtained and the resulting momentum calculated. It is recognized that when a slug of high pressure air is injected into a duct inlet, a series of compression waves proceed down the duct and are reflected as expansion waves from the exit. This wave action continues until the slug of high

pressure air proceeds completely down the duct and out the exit or another slug is injected and a new series of waves begins to propagate.

Figure 1 depicts schematically this wave action within the duct. At time t = 0, a high pressure slug of air is injected at the duct inlet. During this high pressure period, $\frac{\Delta a_i^o}{a_o}$ is a constant greater than zero dependent upon the pressure of the slug.

$$\frac{p_i^o}{p_o} = \left(1 + \frac{\Delta a_i^o}{a_o}\right)^{\frac{2\gamma}{\gamma-1}} \qquad (24)$$

This high pressure air causes a series of compression (ΔP) waves to proceed down the duct and be reflected from the exit at station L as expansion (ΔQ) waves. During this time, β, for a wave to propagate and reflect, the value of ΔP_i remains constant as is indicated in the plot of ΔP_i in Figure 1. If the inlet remains exposed to high pressure air for a time greater than β, another ΔP wave will propagate and be reflected completing a second cycle in period one. When the inlet is then exposed to ambient air, $\frac{\Delta a_i^o}{a_o}$ becomes zero from Equation (24). The propagation and reflection of waves during period two (exposure to ambient air) will continue until the value of ΔP_i has decayed to its initial value in period one. For the example shown in Figure 1, the numerics of which will be discussed subsequently, period two requires five cycles. It will be shown that the number of cycles in each of the exposure periods is a critical factor in the augmentation of an unsteady flow system.

The pressure waves propagate through the duct at a velocity $\frac{dx}{dt} = u \pm a$ where the positive sign corresponds to propagation toward the exit while the negative sign corresponds to propagation toward the inlet. Thus, the total time required for a wave to travel from the inlet to the exit and return is given by

$$\beta = \int_o^L \frac{dx}{u+a} - \int_o^L \frac{dx}{u-a} = \int_o^L \left(\frac{1}{u+a} - \frac{1}{u-a}\right)dx \qquad (25)$$

For the first order analysis to be considered later, the integrand can be expanded in a Taylor's series and terms of second order and higher dropped as follows.

$$\beta = \frac{1}{a_o} \int_o^L \left(1 - \frac{u}{a_o} - \frac{\Delta a}{a_o} + 1 + \frac{u}{a_o} - \frac{\Delta a}{a_o}\right) dx \qquad (26a)$$

$$\beta = \frac{2L}{a_o}\left[1 - \int_o^1 \frac{\Delta a}{a_o}\, d\left(\frac{x}{L}\right)\right] = \beta_o(1 - \Delta\beta) \qquad (26b)$$

$$\text{where} \quad \beta_o \equiv \frac{2L}{a_o} \qquad \Delta\beta = \int_o^1 \frac{\Delta a}{a_o}\, d\left(\frac{x}{L}\right) \qquad (27)$$

Therefore, the lag time, β, illustrated in Figure 1 will be treated as a constant β_o throughout the first order analysis.

It is necessary to point out that when a wave passes through a wave of the opposite kind or through the slug itself in a constant area duct, its slope may be altered slightly but the value of ΔP or ΔQ would remain unchanged. In this analysis, this is true because it is assumed that there is no entropy change of the fluid in the duct. (See

Equations (7) and (8)). Under this constant entropy assumption, the values of ΔP and ΔQ will remain unchanged from the inlet to the exit during one reflection.

In this system, the high pressure air tends to pump low pressure air through the duct thereby decreasing the momentum of the high pressure slug and increasing the momentum of the ambient air pumped into the duct. Hence a transfer of energy from one air mass to another through the action of the pressure waves. It is the amount of ambient air pumped and the associated energy transfer that will determine the effectiveness of the system.

CHAPTER III

UNSTEADY FLOW IN A CONSTANT AREA DUCT

In the preceding chapter, equations were developed to describe the wave motion inside a duct. In this chapter, these equations will be applied to the case of a constant area duct in which the inlet is alternately exposed to high pressure air and ambient air to determine the momentum increase attributed to the wave action within the duct.

It is possible to solve this unsteady flow problem by calculating the momentum of the efflux from the duct exit during the periods of unsteady flow. By determining the relation of the momentum to the ΔP variation and integrating over the periods of flow, the total momentum can be obtained and then compared to the momentum of a comparable steady flow system. The ratio of these momenta is the thrust augmentation attributed to the unsteady flow.

Thus the problem is to now relate ΔP to the momentum in such a manner that it can be integrated in closed form. Due to the complexity of the relations already derived, this is difficult to do without certain simplifying assumptions; however it is possible to obtain an exact solution by numerical-graphical integration. The numerical-graphical integration solution is lengthy and time consuming but offers an exact solution without approximations that will be required for evaluating a closed form approximate analytical expression. For this reason, the numerical-graphical solution will be developed and the results therefrom

presented as a check on the subsequent analytical expression for the same flow problem.

A. Numerical - Graphical Solution

The exact expression of Equation (22) at the inlet station at time, $t + \beta$, is

$$\frac{\gamma+1}{2}\Delta P_i(t+\beta) = -\left[2 - \frac{3-\gamma}{2}\Delta Q_i(t+\beta)\right] + \left\{\left[2 - \frac{3-\gamma}{2}\Delta Q_i(t+\beta)\right]^2 - (\gamma+1)\left[\frac{\gamma+1}{4}\Delta Q_i(t+\beta)^2 + 2\Delta Q_i(t+\beta) + \frac{4}{\gamma-1} - \frac{4}{\gamma-1}(A_i^o)^2\right]\right\}^{\frac{1}{2}} \quad (28)$$

A second expression relating ΔQ_i and ΔP_i is obtained by applying the exit boundary condition and the fact that a wave travels from the inlet to the exit and returns unaltered (except at the exit) in a time period β. This relation can be seen from Figure 1 and is

$$\Delta Q_i(t+\beta) = -\Delta P_i(t) \quad (29)$$

where β in this case can be determined exactly from equation (25) rather than from the first order approximation of Equation (27) for β_o. Substituting Equation (29) into Equation (28) yields

$$\Delta(\Delta P) \equiv \Delta P_i(t+\beta) - \Delta P_i(t) = \frac{4}{\gamma-1}\left\{-1 - \Delta P_i(t) + \left[1 + 2\Delta P_i(t) + 2\left(\frac{\gamma+1}{\gamma-1}\right)\frac{\Delta a_i^o}{a_o} - \frac{\gamma-1}{2}(\Delta P_i(t))^2 + \frac{\gamma+1}{\gamma-1}\left(\frac{\Delta a_i^o}{a_o}\right)^2\right]^{\frac{1}{2}}\right\} \quad (30)$$

With this equation, $\Delta(\Delta P_i)$ can be plotted versus $\Delta P_i(t)$ for various values of $\frac{\Delta a_i^o}{a_o}$. This is illustrated in Figure 2.

From Equations (6) and (19), the change in value of ΔP and ΔQ at the inlet from ambient conditions can be expressed as

$$\Delta P_i = \frac{2}{\gamma-1}\left(\frac{\Delta a_i}{a_o}\right) + \frac{u_i}{a_o} \tag{31}$$

$$\Delta Q_i = \frac{2}{\gamma-1}\left(\frac{\Delta a_i}{a_o}\right) - \frac{u_i}{a_o} \tag{32}$$

Evaluating Equations (31) and (32) at time, $t + \beta$, substituting Equation (29) in (32) and solving the resulting relations simultaneously yields

$$\frac{2}{\gamma-1}\,\frac{\Delta a_i}{a_o}(t+\beta) = \frac{\Delta P_i(t+\beta) - \Delta P_i(t)}{2} = \frac{\Delta(\Delta P_i)}{2} \tag{33}$$

$$\frac{u_i}{a_o}(t+\beta) = \frac{\Delta P(t+\beta) + \Delta P(t)}{2} \tag{34}$$

From Equations (10) and (21), the exit velocity at any instant of time is given by

$$\frac{u_e}{a_o} = \frac{P_e - Q_e}{2} = \frac{\Delta P_e - \Delta Q_e}{2} \tag{35}$$

However since the exit boundary condition demands that $\Delta Q_e = -\Delta P_e$, this reduces to

$$\frac{u_e}{a_o} = \Delta P_e \tag{36}$$

Furthermore since the value of P along the characteristic from the inlet to the exit is constant, it follows that

$$\Delta P_e(t + \frac{\beta}{2}) = \Delta P_i(t) \tag{37}$$

Therefore

$$\frac{u_e}{a_o}(t + \frac{\beta}{2}) = \Delta P_i(t) \tag{38}$$

From the boundary condition that the pressure at the exit must be ambient, it can be said that the density at the exit is equal to ambient density. The total momentum per unit area of the unsteady outflow can be expressed

$$M_T = a_o^2 \int_o^{t_1 \text{ and } t_2} \left[\frac{u_e}{a_o}(t + \frac{\beta}{2})\, \rho_e\right] \frac{u_e}{a_o}(t + \frac{\beta}{2})\, dt =$$

$$a_o^2\, \rho_o \int_o^{t_1 \text{ and } t_2} \left[\Delta P_i(t)\right]^2 dt \tag{39}$$

while the momentum of a steady flow unaugmented system (high pressure air flow only) would be

$$M_{s.s.} = a_o(\text{mass})_{\text{primary}} \left(\frac{u_e}{a_o}\right)_{ss} = a_o(\text{mass})_{\text{primary}}\, \Delta P_{s.s.} \tag{40}$$

The mass of the primary (high pressure) air flow per unit of cross section area is

$$m_p = \int_o^{t_1} \rho_i(t) u_i(t) dt = a_o\, \rho_o \int_o^{t_1} \frac{\rho_i}{\rho_o}(t)\, \frac{u_i}{a_o}(t) dt \tag{41}$$

The inlet velocity is given by Equation (34) and from the equation of state, the ratio of the inlet to ambient density using Equation (33) is

$$\frac{\rho_i}{\rho_o}(t) = \left[\frac{a_i}{a_o}(t)\right]^{\frac{2}{\gamma-1}} = \left[1 + \frac{\Delta a_i(t)}{a_o}\right]^{\frac{2}{\gamma-1}} = \left[1 + \frac{1}{2}\Delta(\Delta P_i)\right] \quad (42)$$

Applying this relation to Equation (41) and substituting into Equation (40) gives the steady state momentum

$$M_{s.s.} = a_o^2 \rho_o \Delta P_{s.s.} \int_o^{t_1} \left[1 + \frac{1}{2}\Delta(\Delta P_i)\right]\left[\frac{\Delta P_i(t+\beta)+\Delta P_i(t)}{2}\right]dt \quad (43)$$

The expression for the thrust augmentation can now be obtained by dividing the unsteady flow momentum of Equation (39) by the steady flow momentum of Equation (43). Since ΔP remains constant for each cycle in periods 1 and 2, the integration in Equations (39) and (43) can be replaced by summations over the appropriate cycles. The corresponding expression for augmentation, λ, is given by

$$\lambda = \frac{M_T}{M_{ss}} = \frac{\sum_{\text{all cycles}} \left(\Delta P_i(t)\right)^2 \beta}{\Delta P_{s.s.} \sum_{\text{cycles in period 1}} \left(1 + \frac{1}{2}\Delta(\Delta P_i)\right)\left[\frac{\Delta P_i(t+\beta)+\Delta P_i(t)}{2}\right]\beta} \quad (44)$$

Since this unsteady flow process involves injecting slugs of high pressure air at regular intervals while the inlet is exposed to ambient air at all other times, the initial condition of period 1 (high pressure air injection) must always correspond to the final condition

of period 2 (exposure to ambient air).

Making use of this boundary condition and the curves of Figure 2, the values of $\Delta P_i(t + \beta)$, $\Delta P_i(t)$, and $\Delta(\Delta P_i)$ can be obtained to compute the augmentation ratio of equation (44).

The method used is an iteration process whereby for a given value of $\frac{\Delta a_i^o}{a_o}$, select an arbitrary value of $\Delta P_i(t)$. Enter Figure 2 with this value of $\Delta P_i(t)$ and read the value of $\Delta(\Delta P_i)$ from the given curve of $\frac{\Delta a_i}{a_o}$. This represents one cycle in Period 1.

$$\Delta P_i(t+\beta) - \Delta P_i(t) = \Delta(\Delta P_i) \tag{45}$$

Calculate $\Delta P_i(t + \beta)$ from Equation (45) and this now becomes $\Delta P_i(t)$ for the next cycle. Repeat this for the number of cycles desired in period 1.

For period 2, $\frac{\Delta a_i^o}{a_o}$ is zero for reasons stated previously therefore the $\frac{\Delta a_i}{a_o} = 0$ curve is utilized for determining ΔP_i for period 2. Enter Figure 2 with the last value of $P_i(t + \beta)$ from period 1 as the first value of $\Delta P_i(t)$ for period 2. From the $\frac{\Delta a_i^o}{a_o} = 0$ curve, determine $\Delta(\Delta P_i)$. From Equation (45) calculate $\Delta P_i(t + \beta)$, then continue this procedure until the last value of $\Delta P_i(t + \beta)$ for period 2 corresponds to the first value of $\Delta P_i(t)$ for period 1. This completes period 2 and begins another period 1 as another slug of high pressure air is injected. This iteration process is quite time consuming in that if the boundary conditions at the end of the iteration do not correspond exactly to the initial values, another arbitrary value of $\Delta P_i(t)$ must be selected and tried until the boundary conditions are satisfied. This

method is illustrated graphically in Figure 1 and a numerical example of the iteration process is presented in Appendix I.

This numerical-graphical solution closely approximates the actual changes that are taking place within the duct and when the values are summed for all of the cycles, the augmentation of the unsteady flow system can be obtained.

Thrust augmentation ratios are calculated for $\frac{\Delta a_i^o}{a_o} = .01, .025, .10$ (i.e., pressure ratios of $\frac{p_i^o}{p_o} = 1.072, 1.188, 1.945$) and for the cycles in period 1 varying from one to six. The results are plotted in Figure 3.

To obtain reasonable accuracy using this method requires a considerable amount of time for each iteration, therefore it is somewhat unwieldly to use. However, it does offer an excellent check on any analytical expression of the same type flow problem. For this reason, the graphical solution is presented to substantiate the approximate analytical expression that is to be developed.

B. Analytical Solution

The analytical development will be based on the same boundary conditions and two periods of flow as were utilized in the graphical solution. The principal difference between the two solutions is that the graphical solution was exact using Equation (22) while the analytical solution will be limited to a first order analysis of Equation (22) in its expanded form and ΔP_i will be assumed to be a continuous function of time and position rather than a step function as seen in Figure 1. Equation (22) to first order in $\frac{\Delta a_i^o}{a_o}$ is

$$\Delta P_i(t+\beta) = -\Delta Q_i(t+\beta) + \frac{4}{\gamma-1}\frac{\Delta a_i^o}{a_o}(t+\beta) - \Delta Q_i^2(t+\beta) \qquad (46)$$

(the final solution will show that ΔQ_i^2 is of the order $\frac{\Delta a_i^o}{a_o}$). Limiting the equation to first order is necessary so that the solution can be integrated in closed form without becoming too complex to handle. It will be shown that limiting this to a first order analysis gives an excellent approximation of the exact solution obtained using the graphical-numerical method for the pressure ranges investigated ($1.072 < \frac{p_i^o}{p_o} < 1.945$).

Applying the β lag time between ΔP_i and ΔQ_i as seen from Figure 1, Equation (46) becomes

$$\Delta P_i(t+\beta) - \Delta P_i(t) = -\Delta P_i^2(t) + \frac{4}{\gamma-1}\frac{\Delta a_i^o}{a_o}(t+\beta) \qquad (47)$$

Now assuming a continuous function rather than the actual step function of Figure 1 and using a Taylor series expansion for $\Delta P_i(t+\beta)$, the approximate expression

$$\Delta P_i(t+\beta) = \Delta P_i(t) + \frac{d\Delta P_i(t)\beta}{dt} + O(\beta^2) \qquad (48)$$

can be introduced. However, since β is small, $\beta^2 << \beta$ and the higher order terms can be dropped in this first order analysis. Also since $\beta = \beta_o(1 - \Delta\beta)$ from Equation (26b), the second order product $\frac{d\Delta P_i}{dt}\beta_o\Delta\beta$ can be dropped giving

$$\Delta P_i(t+\beta_o) = \Delta P_i(t) + \frac{d\Delta P_i(t)}{dt}\beta_o = \Delta P_i(t) + \frac{d\Delta P_i(t)}{dt/\beta_o} \tag{49}$$

Substituting this into Equation (47), it then becomes

$$\frac{d\Delta P_i(t)}{d(t/\beta_o)} = \frac{4}{\gamma-1}\frac{\Delta a_i^o}{a_o} - \Delta P_i^2(t) \tag{50}$$

Integration of this equation yields

$$2\Delta P_i(t) = C_4\left(\frac{1 + Be^{-c_4 t/\beta_o}}{1 - Be^{-c_4 t/\beta_o}}\right) \tag{51}$$

where B is an arbitrary constant and

$$c_4 = \sqrt{\frac{4}{\gamma-1}\frac{\Delta a_i^o}{a_o}} \tag{52}$$

During period 1 when the high pressure slug is injected into the duct at $t = 0$, $\Delta P_{i_1}(t) = \Delta P_{i_1}(0)$ where the subscript 1 represents period one and $\Delta P_i(0)$ represents the initial boundary conditions. Applying this boundary condition to Equation (51), the value of B is determined.

$$B = \frac{\frac{2\Delta P_i(0)}{c_4} - 1}{2\frac{\Delta P_i(0)}{c_4} + 1} \tag{53}$$

Letting $c_4 \frac{t_1}{\beta_o} = \tau_1$, the expression for ΔP_i during period 1 can be written

$$\Delta P_{i_1}(\tau) = \frac{c_4}{2}\left(\frac{1 + Be^{-\tau_1}}{1 - Be^{-\tau_1}}\right) \tag{54}$$

and letting $B = -e^{A}$, Equation (54) further reduces to

$$\Delta P_{i_1}(\tau) = \frac{c_4}{2} \tanh \frac{\tau_1 - A}{2} \tag{55}$$

As stated previously, $\frac{\Delta a_i^o}{a_o} = 0$ during period 2, hence $c_4 = 0$ for this period. From Equation (50), for period 2,

$$\frac{d\Delta P_i(t)}{d(t/\beta_o)} = -\Delta P_i^2(t) \tag{56}$$

which integrates to give

$$\Delta P_{i_2}(t) = \frac{1}{\frac{t_2}{\beta_o} + c_5} \tag{57}$$

When $t = 0$ during period 2 (assuming for convenience that during period 2, time is also counted from zero), $\Delta P_{i_2}(t) = \Delta P_{i_2}(0)$ and letting $\tau_2 = \frac{t_2}{\beta_o}$, $c_5 = \frac{1}{\Delta P_{i_2}(0)}$ and Equation (57) becomes

$$\Delta P_{i_2}(\tau) = \frac{1}{\tau_2 + \frac{1}{\Delta P_{i_2}(0)}} \tag{58}$$

Equations (51) and (58) describe the change of ΔP_i during the periods concerned. Letting subscript "f" denote the end of the

respective periods and considering the boundary conditions prescribed earlier, the ΔP_i relations can be written,

$$\Delta P_{i_1}(\tau_{1_f}) = \Delta P_{i_2}(0) = \frac{c_4}{2}\,\frac{1 + Be^{-\tau_{1_f}}}{1 - Be^{-\tau_{1_f}}} \tag{59}$$

$$\Delta P_{i_2}(\tau_{2_f}) = \Delta P_{i_1}(0) = \frac{1}{\tau_{2_f} + \frac{1}{\Delta P_{i_2}(0)}} \tag{60}$$

The relationship between conditions at the end of period one and the beginning of period two and the converse are indicated in Equations (59) and (60). It must be remembered throughout this analysis that the end of period one marks the beginning of period two and vice versa.

Equations (53), (59), and (60) can be solved simultaneously for B in terms of τ_{1_f} and τ_{2_f}.

$$B = \frac{(4\sinh\frac{\tau_{1_f}}{2} - 2\,\frac{c_4}{2}\,\tau_{2_f}\cosh\frac{\tau_{1_f}}{2}) + \sqrt{(4\sinh\frac{\tau_{1_f}}{2} - 2\,\frac{c_4}{2}\,\tau_{2_f}\cosh\frac{\tau_{1_f}}{2})^2 - 4(\frac{c_4}{2}\,\tau_{2_f})^2}}{2(\frac{c_4}{2}\,\tau_{2_f})\,e^{-\frac{\tau_{1_f}}{2}}} \tag{61}$$

The momentum of the flow during both periods can now be determined by integrating the mass times the velocity over the period of flow. Since the exit boundary conditions stipulate that $\rho_o = \rho_e$, the total momentum outflow per cycle per unit area is

$$M_T = \rho_o \int_o^{t_{1_f}} u_{e_1}^2(t + \tfrac{\beta}{2})dt + \rho_o \int_o^{t_{2_f}} u_{e_2}^2(t + \tfrac{\beta}{2})dt \tag{62}$$

But as was established earlier,

$$u_e^2(t+\tfrac{\beta}{2}) = a_o^2\,\Delta P_e^2\,(t+\tfrac{\beta}{2}) = a_o^2\Delta P_i^2(t) \tag{63}$$

Applying this relationship to the total momentum equation

$$M_T = \rho_o a_o^2\left[\int_o^{t_{1_f}} \Delta P_{i_1}^{\,2}(t)dt + \int_o^{t_{2_f}} \Delta P_{i_2}^{\,2}(t)dt\right] \tag{64}$$

Substituting the expressions for $\Delta P_{i_1}(\tau_1)$ and $\Delta P_{i_2}(\tau_2)$ into Equation (64) and integrating the momentum over the non-dimensional time periods τ_{1_f} and τ_{2_f}, M_T becomes

$$M_T = \rho_o a_o^2\beta_o\left\{\frac{c_4}{2}\left[\frac{\tau_{1_f}}{2} - \frac{e^{\frac{\tau_{1_f}}{2}} + Be^{-\frac{\tau_{1_f}}{2}}}{e^{\frac{\tau_{1_f}}{2}} - Be^{-\frac{\tau_{1_f}}{2}}} + \frac{1+B}{1-B}\right] - \frac{1}{\tau_{2_f} + \frac{1}{\Delta P_{i_2}(0)}} + \Delta P_{i_2}(0)\right\} \tag{65}$$

In order to determine the thrust augmentation effect of the induction of ambient air by the unsteady flow, an expression for the steady state momentum must be derived in terms of ΔP_e and its related forms.

$$M_{s.s.} = (\text{mass})_{\text{primary}}\, u_{e_{s.s.}} \tag{66}$$

Since the primary flow is injected only during period 1,

$$m_p = \text{mass}\ \tau_{1_f} = \int_o^{t_{1_f}} \rho_o u_e(t+\tfrac{\beta}{2})dt \ \text{per unit of cross section area} \tag{67}$$

Since $\frac{u_e(t+\frac{\beta}{2})}{a_o} = \Delta P_e(t+\frac{\beta}{2})$ from Equation (36) and $\Delta P_{e_1}(t+\frac{\beta}{2}) = \Delta P_{i_1}(t)$ from Equation (37), the primary mass flow can be written

$$m_{\tau_{1_f}} = \rho_o a_o \frac{2\beta_o}{c_4} \int_o^{\tau_{1_f}} \Delta P_{i_1}(\tau)\, d\tau \tag{68}$$

Substituting the expression given for $P_{i_1}(\tau)$ from Equation (54) in the above relation and integrating over the applicable time period, τ_{1_f}, yields

$$m_{\tau_{1_f}} = \rho_o a_o \beta_o \ln \left[\frac{\cosh \frac{\tau_{1_f} - A}{2}}{\cosh \frac{A}{2}} \right] \tag{69}$$

The steady state exit velocity, $u_{e_{s.s.}}$, is determined as $\frac{c_4}{2} a_o$ by taking the limit of Equation (54) as $\tau_{1_f} \to \infty$. Applying this value and Equation (69) to Equation (66) gives the steady state momentum.

$$M_{s.s.} = \frac{\rho_o a_o^2 c_4 \beta_o}{2} \ln \left[\frac{\cosh \frac{\tau_{1_f} - A}{2}}{\cosh \frac{A}{2}} \right] \tag{70}$$

Now the augmentation ratio, λ, can be obtained by dividing Equation (65) by Equation (70)

$$\lambda = \frac{M_T}{M_{ss}} = \frac{\frac{1}{2}\left[\frac{\tau_{1_f}}{2} - \frac{e^{\frac{\tau_{1_f}}{2}} + Be^{-\frac{\tau_{1_f}}{2}}}{e^{\frac{\tau_{1_f}}{2}} - Be^{-\frac{\tau_{1_f}}{2}}} + \frac{1+B}{1-B}\right] + \frac{1}{c_4}\left[\Delta P_{i_2}(0) - \frac{1}{\tau_{2_f}}\frac{1}{\Delta P_{i_2}(0)}\right]}{\frac{1}{2}\ln\left[\frac{\cosh\frac{\tau_{1_f}-A}{2}}{\cosh\frac{A}{2}}\right]} \qquad (71)$$

This equation can be further reduced to the concise form

$$\lambda = \frac{\frac{\tau_{1_f}}{2}}{\ln\left[\frac{\cosh\frac{\tau_{1_f}-A}{2}}{\cosh\frac{A}{2}}\right]} = \frac{\frac{\tau_{1_f}}{2}}{\frac{\tau_{1_f}}{2} + \ln\left[\frac{1 - Be^{-\tau_{1_f}}}{1 - B}\right]} \qquad (72)$$

In order to determine the pumping action of this unsteady flow system, it is necessary to evaluate the total mass flow in both periods. The mass flow per cycle per unit area can be written

$$\text{mass}_{\text{Total}} = \rho_o\left[\int_o^{\tau_{1_f}} u_{e_1}\,dt + \int_o^{\tau_{2_f}} u_{e_2}\,dt\right] \qquad (73)$$

Again making use of the relation, $u_e = \Delta P_e$ and the corresponding relations derived earlier, Equation (73) can be written

$$m_T = \rho_o a_o\left[\frac{\beta_o}{c_4}\int_o^{\tau_{1_f}} \frac{c_4}{2}\tanh\frac{\tau_1 - A}{2}\,d\tau_1 + \beta\int_o^{\tau_{2_f}} \frac{1}{\tau_2 + \frac{1}{\Delta P_{i_2}(0)}}\,d\tau_2\right] \qquad (74)$$

Integration and substitution yields

$$m_T = \rho_o a_o \beta_o \left[\ln \frac{\cosh \frac{\tau_{1_f} - A}{2}}{\cosh \frac{A}{2}} + \ln \left(1 + \Delta P_{i_2}(0) \tau_{2_f}\right) \right] \tag{75}$$

Dividing Equation (75) by the primary mass flow expressed by Equation (69) gives the mass flow ratio of the total flow to the primary flow.

$$\frac{m_T}{m_P} = 1 + \frac{\ln \left[1 + \frac{c_4 \tau_{2_f}}{2} \left(\frac{1 + Be^{-\tau_{1_f}}}{1 - Be^{-\tau_{1_f}}} \right) \right]}{\frac{\tau_{1_f}}{2} + \ln \left[\frac{1 - Be^{-\tau_{1_f}}}{1 - B} \right]} \tag{76}$$

With the augmentation ratio and mass flow ratio expressions now available, it is possible to calculate these values for any pressure ratio and given number of cycles in periods 1 and 2. Figure 4 depicts the augmentation ratio curves for values of $\frac{\Delta a_i^o}{a_o}$ of .010, .025, and .100 which correspond to pressure ratios of $\frac{p_i^o}{p_o} = 1.072$, 1.188, and 1.945 respectively. As a comparison of the analytical results with the numerical-graphical solution, Figure 4 also reflects the augmentation ratios determined by the graphical method. It can be seen that for a low number of cycles in period 2, the two curves are in very close agreement and as the number of cycles increase, the error never exceeds 10 per cent even for the higher pressure ratio. The fact that the error becomes significant as the number of cycles in period 2 increases and the pressure ratio increases is a result of limiting the analytical solution to a first order analysis. In actuality the analytical solution can be carried to a higher order, but the additional terms involved

make it difficult to handle the integration without the use of a computer. The curves in Figure 4 bear out the validity of the first order analysis as a good approximation to the exact solution.

It can be shown by application of the continuity and momentum equations that the thrust augmentation ratio of an ideal augmenter is exactly equal to the square root of the mass flow ratio.[4] Since the development in this investigation is not based on an ideal augmenter, it is of interest to note the comparison of the square root of the mass flow ratio to the augmentation ratio as determined by the expressions of Equation (72) and (76). This comparison is indicated in Figure 5a for one and two cycles in period 1 ($\frac{\tau_{1_f}}{\beta_o} = 1$ and 2) with $\frac{\Delta a_i^o}{a_o} = .01$. It can be seen that the square root of the mass flow ratio approximates quite closely the thrust augmentation ratio as derived herein.

Using the square root of the mass flow ratio as the optimum augmentation for a given set of conditions, an augmentation efficiency factor can be defined as

$$\eta = \frac{\frac{M_T}{M_{s.s.}}}{\sqrt{\frac{m_T}{m_{s.s.}}}} \qquad (77)$$

For the values of Figure 5a, the efficiency is plotted in Figure 5b. For the unsteady flow system under study, the efficiency is less than one because the exit velocity is non-uniform in time at the duct exit.

Since the performance of the experimental apparatus in this investigation will be based on the ability of the unsteady flow system to

pump a secondary flow of air, it is of interest at this point to determine what pumping ratio the theory predicts. These ratios of total flow to primary flow are plotted in Figure 6 for $\frac{\Delta a_i^o}{a_o}$ = .01, .025, and .075 for one cycle in period 1.

Because of the excellent comparison of data obtained by use of the analytical expression with the data obtained by the exact numerical-graphical method, it is felt that the first order analytical expression offers a convenient and concise method for evaluating the thrust augmentation and mass flow ratio of any unsteady flow system comparable to the model established for this development.

CHAPTER IV

UNSTEADY FLOW IN A DIVERGING DUCT

The analysis of this chapter will be concerned with the application of the unsteady flow equations of Chapter II to a diverging duct. The basic equations and assumptions used will be the same as those used in the constant area duct development except that the area change term of Equations (5) will be retained.

The effects of divergence will be determined for the two extreme cases of sudden expansion illustrated in Figure 7 rather than for the realistic case of continuous divergence. In Case 1, the divergence is assumed to occur abruptly at the inlet while in Case 2, the divergence occurs abruptly at the exit. These two extremes are selected since the results will establish the performance limits for all physical cases of continuous divergence. Furthermore, this affords simplicity in the analysis by allowing a quasi-steady flow solution (as defined in Chapter II) to be used during the divergence. Thus, wave equation solutions will be required for only the constant area portion of the duct.

Case 1: In Case 1, the inlet flow to "i" followed by the diffusion from "i" to "a" are assumed to occur abruptly as successive quasi-steady flow processes. This is equivalent to evaluating the inlet flow to "a" in a single step independent of the conditions at "i". Therefore, the inlet boundary conditions as utilized in the constant area duct can be applied directly at "a". Downstream of "a", the area remains

constant. Consequently, the constant area solution of Chapter III is directly applicable in this case. The thrust augmentation curves in Figure 5 and the mass flow ratio curves of Figure 6 are therefore applicable to this case. The divergence from "i" to "a" serves only to increase the inflow velocity in comparison with the velocity in the constant area section

Case 2: Assuming that the flow in the duct is of constant entropy, the diffuser flow for quasi-steady conditions can be expressed by Equations (5) written in the form

$$\left(\frac{u + a}{a_o}\right) \frac{dP}{dx} = - \frac{au}{a_o^2} \frac{d \ln \alpha}{dx} \tag{78}$$

$$\left(\frac{u - a}{a_o}\right) \frac{dQ}{dx} = - \frac{au}{a_o^2} \frac{d \ln \alpha}{dx} \tag{79}$$

A simultaneous solution of Equations (31) and (32) yields

$$\frac{a}{a_o} = 1 + \frac{\gamma - 1}{2} \left(\frac{\Delta P + \Delta Q}{2}\right) \tag{80}$$

$$\frac{u}{a_o} = \frac{\Delta P - \Delta Q}{2} \tag{81}$$

Substitution of these expressions into Equations (78) and (79) gives

$$\left[\frac{\Delta P - \Delta Q}{2} + 1 + \frac{\gamma-1}{2} \left(\frac{\Delta P + \Delta Q}{2}\right)\right] \frac{d\Delta P}{dx} = - \frac{au}{a_o^2} \frac{d \ln \alpha}{dx} \tag{82}$$

$$\left[\frac{\Delta P - \Delta Q}{2} - 1 - \frac{\gamma-1}{2} \left(\frac{\Delta P + \Delta Q}{2}\right)\right] \frac{d\Delta Q}{dx} = - \frac{au}{a_o^2} \frac{d \ln \alpha}{dx} \tag{83}$$

Since the right hand side of Equations (82) and (83) are identical, they can be equated as follows.

$$\left[\frac{\Delta P-\Delta Q}{2} + 1 + \frac{\gamma-1}{2}\left(\frac{\Delta P+\Delta Q}{2}\right)\right]\frac{d\Delta P}{dx} = \left[\frac{\Delta P-\Delta Q}{2} - 1 - \frac{\gamma-1}{2}\left(\frac{\Delta P+\Delta Q}{2}\right)\right]\frac{d\Delta Q}{dx} \quad (84)$$

This relation between ΔP and ΔQ can be rearranged into an integrable form as

$$\left[1 + \frac{\gamma-1}{2}\left(\frac{\Delta P+\Delta Q}{2}\right)\right] d(\Delta P+\Delta Q) = -\left(\frac{\Delta P-\Delta Q}{2}\right) d(\Delta P-\Delta Q) \quad (85)$$

Integration of Equation (85) then yields

$$\Delta Q^2 + \frac{8}{\gamma+1}\left(1 + \frac{\gamma-3}{4}\Delta P\right)\Delta Q + \frac{8}{\gamma+1}\left(\Delta P + \frac{\gamma+1}{8}\Delta P^2 - C\right) \quad (86)$$

where C is the arbitrary constant of integration.

ΔP and ΔQ can be evaluated from Equation (86) to second order in ΔP and ΔQ by using a Taylor's series expansion. The result is

$$\Delta Q = -(\Delta P^2 + \Delta P) + C \qquad \Delta P = -(\Delta Q^2 + \Delta Q) + C \quad (87)$$

The relationships between ΔP at the diffuser inlet and exit and ΔQ at the diffuser inlet and exit can now be determined from Equations (82), (83), and (87). Substitution of Equation (87) into Equation (82) gives the differential equation relating ΔP to the area change in the diffuser.

$$\frac{2(1 + \Delta P)d\Delta P}{\Delta P^2 + 2\Delta P - C} = -d \ln \alpha \quad (88)$$

Letting "b" represent the beginning of the diverging section and "e" represent the end of the diverging section as shown in Figure 7, Equation (88) can be integrated across this distance with the result.

$$\Delta P_e^{\,2} + 2\Delta P_e - C = \frac{\alpha_b}{\alpha_e} \left(\Delta P_b^{\,2} + 2\Delta P_b - C\right) \tag{89}$$

Equation (89) can be expanded by a Taylor's series and to second order in ΔP is

$$\Delta P_e = \frac{1}{2} C \left(1 - \frac{\alpha_b}{\alpha_e}\right) + \Delta P_b \frac{\alpha_b}{\alpha_e} \left(1 + \frac{\Delta P_b}{2}\right) \tag{90}$$

Similarly from Equations (83), and (87), the following relation between ΔQ_e and ΔQ_b is obtained.

$$\Delta Q_e = \frac{1}{2} C \left(1 - \frac{\alpha_b}{\alpha_e}\right) + \Delta Q_b \frac{\alpha_b}{\alpha_e} \left(1 + \frac{\Delta Q_b}{2}\right) \tag{91}$$

The boundary condition at the diffuser exit is $\Delta P_e = -\Delta Q_e$ as derived in Chapter II. The arbitrary constant of integration contained in Equations (90) and (91) can now be determined by applying this boundary condition to Equations (87). This gives $C = \Delta P_e^2 = \Delta Q_e^2$.

From Equation (87), the relation for ΔQ evaluated at station "b" becomes

$$\Delta Q_b = -(\Delta P_b^2 + \Delta P_b) + \Delta P_e^2 \tag{92}$$

From Equation (90), ΔP_e to terms of order ΔP^2 becomes

$$\Delta P_e^2 = \Delta P_b^2 \left(\frac{\alpha_b}{\alpha_e}\right)^2 \tag{93}$$

The final relation between ΔQ_b and ΔP_b can be obtained by substituting Equation (93) into Equation (92).

$$\Delta Q_b = -\Delta P_b \left\{ 1 + \Delta P_b \left[1 - \left(\frac{\alpha_b}{\alpha_e}\right)^2 \right] \right\} \tag{94}$$

It now becomes necessary to relate conditions at "i" to the conditions established at "b". Using the lag time, β, and the corresponding wave relations illustrated in Figure 1 for the constant area duct, ΔQ_i and ΔQ_b are related as follows.

$$\Delta Q_i(t + \beta) = \Delta Q_b \left(t + \frac{\beta}{2}\right) \tag{95a}$$

$$\Delta P_b\left(t + \frac{\beta}{2}\right) = \Delta P_i(t) \tag{95b}$$

Evaluation of Equation (94) at time, $t + \frac{\beta}{2}$, and substitution of Equations (95) therein gives

$$\Delta Q_i(t + \beta) = -\Delta P_i(t) \left\{ 1 + \Delta P_i(t) \left[1 - \left(\frac{\alpha_b}{\alpha_e}\right)^2 \right] \right\} \tag{96}$$

Finally, the inlet boundary condition for quasi-steady inlet flow derived in Chapter II can be applied to the inlet of Case 2 which is a constant area section. From Equation (46), this boundary condition is

$$\Delta P_i = -\Delta Q_i + \frac{4}{\gamma - 1} \frac{\Delta a_i^{\,o}}{a_o} - \Delta Q_i^{\,2} \tag{97}$$

Evaluating this boundary condition at time, $t + \beta$, and substituting Equation (96) in Equation (97) yields

$$\Delta P_i(t+\beta) = -\Delta P_i(t)\left\{1 + \Delta P_i(t)\left[1 - \left(\frac{\alpha_b}{\alpha_e}\right)^2\right]\right\} + \frac{4}{\gamma-1}\frac{\Delta a_i^o}{a_o} - \Delta P_i^2(t)\left\{1 + \Delta P_i(t)\left[1 - \left(\frac{\alpha_b}{\alpha_e}\right)^2\right]\right\}^2 \qquad (98)$$

By limiting this expression to terms of order ΔP^2, and applying the differential relation of Equation (49), Equation (98) becomes

$$\frac{d\Delta P_i(t)}{dt}(\beta_o) = \Delta P_i(t+\beta_o) - \Delta P_i(t) = \frac{4}{\gamma-1}\frac{\Delta a_i^o}{a_o} - \Delta P_i^2(t)\left(\frac{\alpha_b}{\alpha_e}\right)^2 \qquad (99)$$

Equation (99) is the final differential equation for ΔP_i. Through the same analysis used for the constant area duct solution, it can be integrated to give for period 1,

$$\Delta P_{i_1}(t) = \frac{c_4}{2}\,\frac{1 + Be^{-\tau_1}}{1 - Be^{-\tau_1}} \qquad (100)$$

where

$$c_4 = 2\sqrt{\frac{4}{\gamma-1}\frac{\Delta a_i^o}{a_o}}\left(\frac{\alpha_e}{\alpha_b}\right)$$

$$\tau_1 = c_{4_a}\frac{t_1}{\beta_o} \qquad c_{4_a} = c_4\left(\frac{\alpha_b}{\alpha_e}\right)^2$$

For period 2, Equation (99) becomes

$$\Delta P_{i_2} = \frac{1}{\tau_2 + \frac{1}{\Delta P_{i_2}(0)}} \tag{101}$$

where

$$\tau_2 = \left(\frac{\alpha_b}{\alpha_e}\right)^2 \frac{t_2}{\beta_o}$$

By use of the boundary condition that ΔP at the beginning of period 1 must correspond to ΔP at the end of period 2 and the converse, the expression for B can be derived and is the same as that given in Equation (61).

In order to calculate the exit momentum and mass flow ratio for the diverging duct, the ΔP_i relations for the two periods must be transferred to the exit. This is accomplished through the use of Equation (93). Since station "b" corresponds to the inlet of the diffuser section and is of the same area as the duct inlet, Equation (93) can be written

$$\Delta P_e = \Delta P_i \left(\frac{\alpha_b}{\alpha_e}\right) \tag{102}$$

Applying this relation to Equations (100) and (101), they become

$$\Delta P_{e_1} = \frac{c_4}{2} \frac{\alpha_b}{\alpha_e} \tanh \frac{\tau_1 - A}{2} \quad \text{where } -e^A = B \tag{103}$$

$$\Delta P_{e_2} = \frac{\alpha_b}{\alpha_e} \left(\frac{1}{\tau_2 + \frac{1}{\Delta P_{i_2}(0)}}\right) \tag{104}$$

Except for the area term, $\frac{\alpha_b}{\alpha_e}$, these relations are identical to those derived for the constant area duct. Hence the solution for the diverging duct augmentation ratio and mass flow rate reduces to the constant area solution except for the area ratio terms which are introduced in the new values of c_4, τ_1, and τ_2.

The integration of the exit velocity over the time periods to obtain the total momentum and mass flow will not be repeated here since it follows the same procedure used in the solution derived in Chapter III.

In summary the diverging duct augmentation ratio is

$$\lambda = \frac{M_T}{M_{s.s.}} = \frac{\frac{\tau_{1_f}}{2}}{\frac{\tau_{1_f}}{2} + \ln\left(\frac{1 - Be^{-\tau_{1_f}}}{1 - B}\right)} \tag{105}$$

and the mass flow ratio is

$$\frac{m_T}{m_P} = 1 + \frac{\ln\left[1 + \frac{c_4}{2}\tau_{2_f}\left(\frac{1 + Be^{-\tau_{1_f}}}{1 - Be^{-\tau_{1_f}}}\right)\right]}{\frac{\tau_{1_f}}{2} + \ln\left(\frac{1 - Be^{-\tau_{1_f}}}{1 - B}\right)} \tag{106}$$

where the relations for B, c_4, τ_1, and τ_2 as a function of area ratio and $\frac{\Delta a_i^{\,o}}{a_o}$ have been given in the development.

Curves for the augmentation ratios for the two cases of the diverging duct are presented in Figure 8 $\left(\frac{\Delta a_i^{\,o}}{a_o} = .01 \text{ and } \frac{t_1}{\beta_o} = 1 \text{ and } 2\right)$. It

will be noted that the performance obtained by diverging the duct at the exit is improved somewhat over the inlet divergence configuration. The performance for the realistic case of continuous divergence from the inlet to the exit should fall between these two extreme cases. However it is apparent that in such a case, the theoretical improvement is only marginal. In addition to this marginal increase in performance due to divergence, it is believed that for any practical design, the inflow conditions and therefore, the augmentation would be substantially improved due to the increase of the inflow velocity. Diffusion due to divergence would undoubtedly offset some of this advantage.

CHAPTER V

EXPERIMENTAL INVESTIGATION

As in any engineering development, it is desirable to incorporate the theory of an analysis into a functional apparatus as a check on its validity. In some cases, a design may precede the theory under which it operates but ultimately the theory will influence refinements of the design for optimum performance and utilization.

For this investigation, a test apparatus used by Lockheed-Georgia Co. for similar experiments was modified to conform to the conditions and assumptions set forth in the theoretical analysis.

A. Equipment and Test Installation

Figure 9 shows a schematic outline of the test installation. High pressure air from two 1000 cubic foot 125 psi. stagnation tanks was reduced to the desired test pressures through a single stage pressure regulator thus maintaining a nearly constant pressure at the test section. This air was piped to the test apparatus through a four inch line with a two inch orifice plate installed at the 100 inch station. Such positioning of the orifice plate insured developed flow and accurate metering.[8] A chromel alumel thermocouple was inserted in the pipe twelve inches upstream of the orifice plate for the purpose of measuring air temperature.

After passing through the orifice plate, the high pressure air was then piped into the test apparatus, a cross-section of which is

shown in Figure 10. The test apparatus consists of a cylindrical chamber fitted on both ends with rotating disks. As depicted in Figures 10 and 11, one disk is slotted to allow passage of the high pressure primary air flow. Details of the slots and the test apparatus are shown clearly in Figure 12. The primary air flow then passes through the slots and out the augmenter duct which mounts on the end of the cylindrical chamber. The augmenter duct is fitted with a 2.75 inch radius bellmouth to turn the secondary air flow smoothly into the duct.

In order to measure the amount of secondary or ambient air being pumped into the duct, a large air tight box as shown in Figure 13 was constructed to contain the entire test apparatus. Any secondary air pumped through the duct was then measured by use of a 6 inch end orifice plate mounted on a 24 inch secondary flow pipe which exposed the interior of the box to ambient air. The reason for using such a large secondary flow pipe and orifice plate was to hold the pressure drop across the plate to a minimum thus keeping conditions in the box and consequently at the bellmouth inlet very near ambient.

As can be seen in Figures 10 and 13, a small electric motor mounted on the shaft of the test apparatus provided for the disk rotation. Rotation speed was controlled through a variable transformer in series with the power line to the motor. A direct reading tachometer was fitted to the rear of the motor to determine rotation speed.

In order for the apparatus to approximate the conditions set forth in the theory, the cross sectional area of the duct was subdivided into many smaller ducts by the insertion of separator vanes made of 1/8 inch aluminum. These vanes extended the length of the duct and were

mounted 20° apart on a wooden center core as shown in Figure 14. By removing every other vane, spacing could be increased to 40°. The vanes themselves did not extend into the bellmouth inlet shown in Figure 10.

Duct length was varied by the use of ducts 23, 8.4 and 4 inches in length that could be fitted to the back side of the bellmouth. The 3.5 inch bellmouth inlet length shown in Figure 8 is not considered part of the duct length, L.

The orifice plates, their locations and related pressure taps were all designed according to A.S.M.E. (American Society of Mechanical Engineers) standard flow measurement specifications.[8,9] In addition to pressure taps for flow measurement, taps were located in the cylindrical section of the augmenter to determine disk pressure (Figure 12). Upstream conditions of the secondary flow lines were considered ambient.

During the test runs, pressures at all taps were simultaneously measured by the use of pressure transducers and recorded by a Heiland Oscillograph. The instrumentation is depicted in Figure 13.

B. Design of Experimental Apparatus

Based on the theory utilized in the analytical development, it was required that a high pressure slug of air be injected into the duct followed by a period of inlet exposure to ambient air. The test apparatus on loan from Lockheed provided such a situation. As the disk rotated, the slots would allow high pressure air to enter part of the duct. As the slot moved further around, the high pressure air would be cut off over that part of the duct and the inlet would then be exposed to ambient air. With the separator vanes subdividing the large duct

into a number of smaller ducts, the flow became similar to that prescribed in the theory.

In order to design a system for optimum performance based on the theory, three principal parameters must be considered. These are: (1) the width, positioning and shape of the rotating disk slots; (2) speed of rotation; (3) duct length. These parameters are all related through $\frac{t_1}{\beta_o}$, $\frac{t_2}{\beta_o}$, and the primary mass flow. Since $\beta_o = \frac{2L}{a_o}$ and the primary mass flow is determined by the pressure ratio and the values of $\frac{t_1}{\beta_o}$ and $\frac{t_2}{\beta_o}$, the value of the duct length can then be determined. The time length of period 1 and period 2 is determined from the rotation speed and the slot size. The three parameters cited are interdependent and all must be considered for any specific design performance.

Since the 13° slots shown in Figure 11 were already cut in the disk, only the parameters of speed and duct length were varied during this investigation.

Duct lengths, L, of 23, 8.4, and 4 inches were selected so as to have some comparison of performance between a long and short duct and the associated friction effects. For two tests, the duct inlet was modified so as to station the duct itself 1.5 inches from the disk face rather than the 4.5 inches as shown in Figure 10.

It was not possible to arrive at a design rotation speed since the slots were already fixed in position and the ratio of slot width to the solid disk width remained constant regardless of speed. Thus it was decided to conduct tests at varied speeds over a wide range of pressure ratios and observe the performance as the speed varied.

In an effort to contain the wave action within a small cross section of the duct, the separator vanes as shown in Figure 14 were designed to subdivide the large cross sectional area of the duct into eighteen smaller ducts. Tests could then be conducted with and without vanes to determine the effect of reducing the duct area.

C. Procedure

Following the installation of the test apparatus and calibration of the recording instruments, the disk slots were sealed and the apparatus was calibrated for leakage. The augmenter assembly was installed in the air tight box in such a manner that the primary flow leakage would be directed out the rear of the box around the motor and would not flow into the box itself and interfere with the measurement of secondary flow (see Figure 13). Leakage flow is plotted in Figure 15 for the range of test pressure ratios.

Initial tests were conducted using the 23 inch duct with the bellmouth positioned one inch from the disk face. Rotation speed was varied from zero to 6000 RPM while the ratio of the primary air pressure to ambient pressure was varied from 1.0 to 1.4.

The duct was then shortened to 8.4 inches and tested under the same conditions as above. The internal separator vanes were then installed in this duct and the tests repeated for the eighteen vane configuration and a nine vane configuration.

From Figure 10 it can be seen that the actual constant area duct begins 3.5 inch from the bellmouth inlet. It was felt that this distance being quite large compared to the average slot width of 0.4 inch might be detrimental to performance. Therefore, the inlet was modified slightly to

bring the duct to a position one inch from the bellmouth inlet. The bellmouth inlet was then positioned one-half inch from the disk face. With the 8.4 inch duct repositioned, tests were then conducted over the same speeds and pressure ratios used in the initial tests.

The duct was then shortened to four inches and tested with the modified inlet positioned 1/2 inch from the disk face as before. This test was conducted with nine separator vanes in the duct.

D. Results

The primary air flow rate for all tests proved to be the same and was dependent only on pressure ratio and leakage. The primary flow and leakage flow rates are plotted in Figure 15.

The pumping ratio of the augmenter apparatus is specified as the ratio of the total duct outflow to the primary air flow and for the four ducts tested is plotted in Figures 16, 17, 18, and 19. Data points for the disk rotation condition are for the rotative speed which gave the best pumping action. It was observed that the pumping action was best at speeds between 2000-2500 rpm in all cases. Speeds higher or lower than this range caused the flow rate of secondary air to decrease. This is illustrated by the typical plot of pumping ratio vs. RPM shown in Figure 20.

As can be seen from Figure 16, the no rotation pumping ratio was almost equal to the rotation pumping ratio for the 23 inch duct. Since the length to diameter ratio was 3.5 for this duct, the no rotation condition was probably approximating the conditions of a steady flow, viscous type augmenter.

A graphical comparison of the augmenter performance for all configurations tested is shown in Figure 21. It will be noted that the best performance was obtained using the 8.4 inch duct and the 2.75 inch radius bellmouth positioned one inch from the disk face. The calculated theory for this configuration is reflected along with the actual performance in Figure 17. A sample of the numerical calculations used to establish the theoretical performance of this configuration at the optimum speed of rotation is presented in Appendix III. In making the theoretical calculations, it was necessary to iterate to an optimum RPM. In all cases, this optimum RPM was found to be in the range of 2000-2500. This speed range is in good agreement with the experimental values.

From Figure 17, it can be seen that the performance of the augmenter with the separator vanes installed in the duct did not improve over the no separator vane configuration. This is probably attributed to large friction losses in the subdivided duct since the duct wetted area is increased by a factor of five when the eighteen internal vanes are installed. Thus, the pumping action probably did increase but the associated increase in friction losses offset this improvement.

The overall performance of the system was somewhat less than what the theory predicted. However this can be attributed to factors which were either uncontrolled or not considered in this investigation. The design of the slots in the disk (i.e., shape, lip radius, etc.) and the duct inlet are both quite important and should be investigated further to determine their effect on performance. It is highly probable that diverging the duct would improve the inlet conditions and consequently the augmenter performance as discussed in Chapter IV.

Diffusion of the high pressure air as it flows from the disk slots to the duct inlet would vary the times of periods 1 and 2 when evaluating the theoretical performance. As can be seen from Figure 3, when the time in period 1 increases, the performance drops off sharply. Diffusion could well account for the fact that the experimental apparatus did not perform as well as predicted by the theory. Assuming that the high pressure air diffused to twice its exit width before it entered the augmenting duct, the theoretical pumping ratio for the 8.4 inch duct would be reduced considerably as shown in Figure 17. Thus the actual performance achieved in the experiment was between the predicted theoretical pumping ratio and the theoretical pumping ratio evaluated if the air were diffused to twice its exit width.

For all configurations tested, the experiments did point out that better performance could be expected at low pressure ratios as is borne out by the theory. Also, the unsteady flow induced by the disk rotation did improve the pumping ratio as compared to the pumping ratios obtained during the no rotation tests.

CHAPTER VI

CONCLUSIONS

The problem of thrust augmentation utilizing unsteady flow in a constant area duct has been solved by use of the wave equations. This method of analysis closely approximates the physical situation and provides an accurate means of evaluating the pressure and velocity within the duct once the wave relations are established.

The exact numerical-graphical solution of the wave equation was evaluated for a constant area duct but required a considerable amount of time to achieve accuracy in the iteration process.

The associated analytical solution of the problem is a concise expression yielding results within at least ten per cent of the exact solution for primary flow pressure ratios up to 1.945. The accuracy of this solution could be improved further by introducing the higher order terms which were dropped from the expression for simplification.

For any given flow conditions, thrust augmentation was found to be within at least five per cent of the ideal value which is equal to the square root of the mass flow ratios. For fixed periods of unsteady flow, augmentation increased with a decrease in pressure of the high pressure flow. Increasing the period of inlet exposure to ambient air and decreasing the period of exposure to the high pressure flow both increased the augmentation.

The analytical solution for thrust augmentation due to unsteady

flow in a diverging duct showed that the theoretical improvement over the constant area solution is only marginal. It is believed however that for any practical design, divergence would improve the inflow conditions. The augmentation would then be improved due to an increase in the inflow velocity. This velocity increase would allow the primary air to enter the duct quicker and preclude spillage at the inlet.

The experimental investigation proved that the performance of the tested apparatus was improved by the induced unsteady flow as compared to performance of the same system under steady flow conditions. Results indicated that performance decreased as the pressure of the primary air flow increased. This characteristic of the system was borne out by the theory.

Although the performance achieved in the tests did not equal that predicted by the theory, the fact that secondary flow was pumped indicates that the system has potential as a thrust augmenter. The optimum performance disk rotation speed arrived at during the experiments corresponded to that determined by the theoretical analysis.

Continued testing with refinements in design of the system should improve the performance considerably. Factors such as friction effects, diffusion of the high pressure flow and secondary flow inlet position affect the performance and should be incorporated into any subsequent analysis. Additionally, specific attention should be directed towards design of the slots in the rotating disk.

A P P E N D I C E S

APPENDIX I

EXAMPLE NUMERICAL-GRAPHICAL SOLUTION

For this example, a pressure ratio of 1.188 corresponding to $\frac{\Delta a_i^o}{a_o} = .025$ will be used for two cycles in period 1. Following the procedure outlined in Chapter III, an initial arbitrary value of $\Delta P_i(t) = .140$ is selected. Entering Figure 2 with $\Delta P_i(t) = .140$, the value of $\Delta(\Delta P_i)$ for $\frac{\Delta a_i^o}{a_o} = .025$ is .193. Using Equation (45), $\Delta P_i(t + \beta) = .333$. Since two cycles are desired in period 1, use .333 as $\Delta P_i(t)$ for the next cycle. Entering Figure 2 with this value and reading from the $\frac{\Delta a_i^o}{a_o} = .025$ curve, $\Delta(\Delta P_i) = .102$. Again using Equation (45), $\Delta P_i(t + \beta) = .435$. This completes period 1. The number of cycles desired in period 1 is determined by the time of exposure of the inlet to the high pressure air. For this example, two cycles are used arbitrarily.

For period 2, begin with $\Delta P_i(t) = .435$ which was the final value from period 1. Entering Figure 2 with this value, read from the $\frac{\Delta a_i^o}{a_o} = 0$ curve that $\Delta(\Delta P_i) = -.138$. $\Delta P_i(t + \beta) = .297$ using Equation (45). This procedure is repeated for as many cycles as it takes for $\Delta P_i(t + \beta)$ to become equal to the initial value of $\Delta P_i(t)$ in period 1 which was .140. From the table of the complete iteration, it is seen that it takes five cycles in period 2 to get matching boundary conditions.

Iteration Values

$\Delta P_i(t)$	$\Delta(\Delta P_i)$	$\Delta P_i(t + \beta)$	Cycles	Period
.140	.193	.333		1
.333	.102	.435	2	
.435	-.138	.297		2
.297	-.070	.227		
.227	-.040	.187		
.187	-.027	.160		
.160	-.020	.140	5	

$\Delta P_{s.s.}$ is the value of $\Delta P_i(t)$ for which $\frac{\Delta a_i^o}{a_o} = .025$ and $\Delta(\Delta P_i) = 0$. From Figure 2, $\Delta P_{s.s.} = .50$. Applying Equation (44) and using the values obtained above in the summation, the resulting augmentation ratio is

$$\lambda = \frac{M_{u.s.}}{M_{s.s.}} = \frac{.5197}{(.50)(.6635)} = 1.57.$$

This value is then plotted on Figure 3 in its appropriate position for the number of cycles in period 2 and the given pressure ratio.

APPENDIX II

THE LIMITING CASE OF THE CONSTANT AREA DUCT ANALYTICAL SOLUTION

The limiting case of augmentation for a constant area duct can be determined by allowing the term $\frac{\Delta a_i^o}{a_o}$ to go to zero in the augmentation ratio expression found in Equation (72).

$$\lambda = \frac{\frac{\tau_{l_f}}{2}}{\frac{\tau_{l_f}}{2} + \ln \frac{1 - Be^{-\tau_{l_f}}}{1 - B}} \tag{107}$$

As $\frac{\Delta a_i^o}{a_o} \rightarrow 0$, using the Taylor's series expansion for $e^{-\tau_{l_f}} = e^{-\sqrt{\frac{4}{\gamma-1}} \frac{\tau_{l_f}}{\beta_o}}$

$$\frac{1 - Be^{-\tau_{l_f}}}{1 - B} \rightarrow \frac{1 - B(1 - \tau_{l_f})}{1 - B} = 1 + \frac{B\tau_{l_f}}{1 - B} \tag{108}$$

and

$$\ln \left(1 + \frac{B\tau_{l_f}}{1 - B}\right) \rightarrow \frac{B\tau_{l_f}}{1 - B} \tag{109}$$

hence the augmentation ratio approaches

$$\lambda \rightarrow \frac{1 - B}{1 + B} \tag{110}$$

It now remains to examine the expression for B and determine its limit as $\frac{\Delta a_i^o}{a_o}$ goes to zero. From Equation (61),

$$B = \frac{-4\sinh\frac{\tau_{1_f}}{2} - 2\frac{c_4}{2}\tau_2\cosh\frac{\tau_{1_f}}{2} + \sqrt{\left(-4\sinh\frac{\tau_{1_f}}{2} - 2\frac{c_4}{2}\tau_2\cosh\frac{\tau_{1_f}}{2}\right)^2 - 4\left(\frac{c_4}{2}\tau_{2_f}\right)^2}}{2\left(\frac{c_4}{2}\tau_{2_f}\right)e^{-\tau_{1_f}/2}} \qquad (111)$$

For the limiting case, $\sinh\frac{\tau_{1_f}}{2} \rightarrow \frac{\tau_{1_f}}{2}$, $\cosh\frac{\tau_{1_f}}{2} \rightarrow 1.0$ and $e^{-\tau_{1_f}/2} \rightarrow \left(1 - \frac{\tau_{1_f}}{2}\right)$. Applying these relations to B in Equation (111) and expanding, B becomes

$$B = -1 + \frac{2t_1}{t_2}\left(\sqrt{1 + \frac{t_{2_f}}{t_{1_f}}} - 1\right) \qquad (112)$$

Substituting this expression into Equation (110), the limiting case of the augmentation ratio is

$$(\lambda)_{limit} = \frac{2 - 2\frac{t_{1_f}}{t_{2_f}}\left(\sqrt{1 + \frac{t_{2_f}}{t_{1_f}}} - 1\right)}{2\frac{t_{1_f}}{t_{2_f}}\left(\sqrt{1 + \frac{t_{1_f}}{t_{1_f}}} - 1\right)} \qquad (113)$$

This equation is plotted in Figure 4 and it will be noted that it is the upper limit for the plots of augmentation ratios determined by the graphical integration method and the analytical expression.

APPENDIX III

TEST APPARATUS THEORETICAL PERFORMANCE CALCULATIONS

The calculation of the theoretical performance of the test apparatus is based on the primary mass flow that passes through the slots in the disk. This mass is related to the times in period one and period two through Equation (69).

$$m_P = \rho_o a_o \beta_o \ln\left(\frac{\cosh \frac{\tau_{1_f} - A}{2}}{\cosh \frac{A}{2}}\right) \qquad (69)$$

Performance will be evaluated for the 8.4 inch duct at a pressure ratio of 1.188 which corresponds to a $\frac{\Delta a_i^o}{a_o}$ of .025. From Equation (52), c_4 for this case is equal to 1.

The theoretical mass flow is determined by the velocity of the high pressure air through the slot and the average width of the slot. The cross section shown in Figure 22 indicates the flow pattern of the high pressure air. The average width of the slot is 0.4 inch and assuming a flow coefficient, c, of 0.6, the average width through which the flow actually passes is .24 inch. The Mach number corresponding to the pressure ratio above is 0.51 and using 1116 feet per second as the speed of sound, the velocity, u, through the slot is 570 feet per second.

For a rotation speed of 2500 RPM, the average tangential velocity, v, of the slot is 40.75 feet per second. At this speed of rotation and for the velocity of the high pressure air through the slot, the thickness of

the slug of air passing through the slot is

$$y = \frac{w(c)(u)}{v} = \frac{(.4)(.6)(570)}{40.75} = 3.36 \text{ in.}$$

Since Equation (69) was developed as mass flow per unit of cross section area, m_p is equal to the depth of the slug times the density. This establishes the left hand side of Equation (69).

β_o can be calculated using Equation (27) as follows.

$$\beta_o = \frac{2L}{a_o} = \frac{2(8.4)}{(12)(1116)} = .001252 \text{ sec.}$$

Equation (69) now reduces to

$$3.36 = .001252 \ln\left(\frac{\cosh \frac{c_4 \frac{t_{1_f}}{\beta_o} - A}{2}}{\cosh \frac{A}{2}}\right)$$

where A can be determined from Equation (61).

For the double slotted disk, another slug of high pressure air will be injected into the inlet in 1/2 of one revolution. Hence the total time for period one and period two is the time for the disk to make 1/2 of one revolution. This time divided by β_o for 2500 rpm is

$$\frac{t_1}{\beta_o} + \frac{t_2}{\beta_o} = \frac{60}{2(2500)(.001252)} = 9.57$$

Using the two equations above which are both in terms of $\frac{t_1}{\beta_o}$ and $\frac{t_2}{\beta_o}$, values

can be determined for $\frac{t_1}{\beta_o}$ and $\frac{t_2}{\beta}$. For optimum performance, $\frac{t_1}{\beta_o}$ should be an even number thus allowing for wave reflections to be completed before period two begins.

For this configuration and RPM, $\frac{t_1}{\beta_o}$ is equal to one and $\frac{t_2}{\beta_o}$ is 8.56. These values satisfy both equations simultaneously, therefore they represent the theoretical values of $\frac{t_1}{\beta_o}$ and $\frac{t_2}{\beta_o}$ to be applied to the augmentation ratio Equation (72) to determine the theoretical performance of the system. Applying these values to Equation (72) yields an augmentation ratio of 2.6 which when squared gives the theoretical pumping ratio of 6.75 which is plotted in Figure 17. The augmentation ratio squared is used here rather than the mass flow ratio because it was shown that theoretically the two differ slightly and the lower value is assumed to be more near the expected pumping rate.

The method used here to determine the theoretical values of $\frac{t_1}{\beta_o}$ and $\frac{t_2}{\beta_o}$ requires iteration around the rotation speed and $\frac{t_2}{\beta_o}$ to arrive at values of $\frac{t_1}{\beta_o}$ and $\frac{t_2}{\beta_o}$ which will satisfy the two equations simultaneously. However for all points checked by this method, the iteration closed rapidly on a solution using rotation speeds in the range 2000-2500 RPM which were the speeds that gave the best experimental performance.

If diffusion is considered in the theoretical problem, the same procedure is used except that the slug width is assumed to be greater by the amount of diffusion being considered.

APPENDIX IV

FIGURES

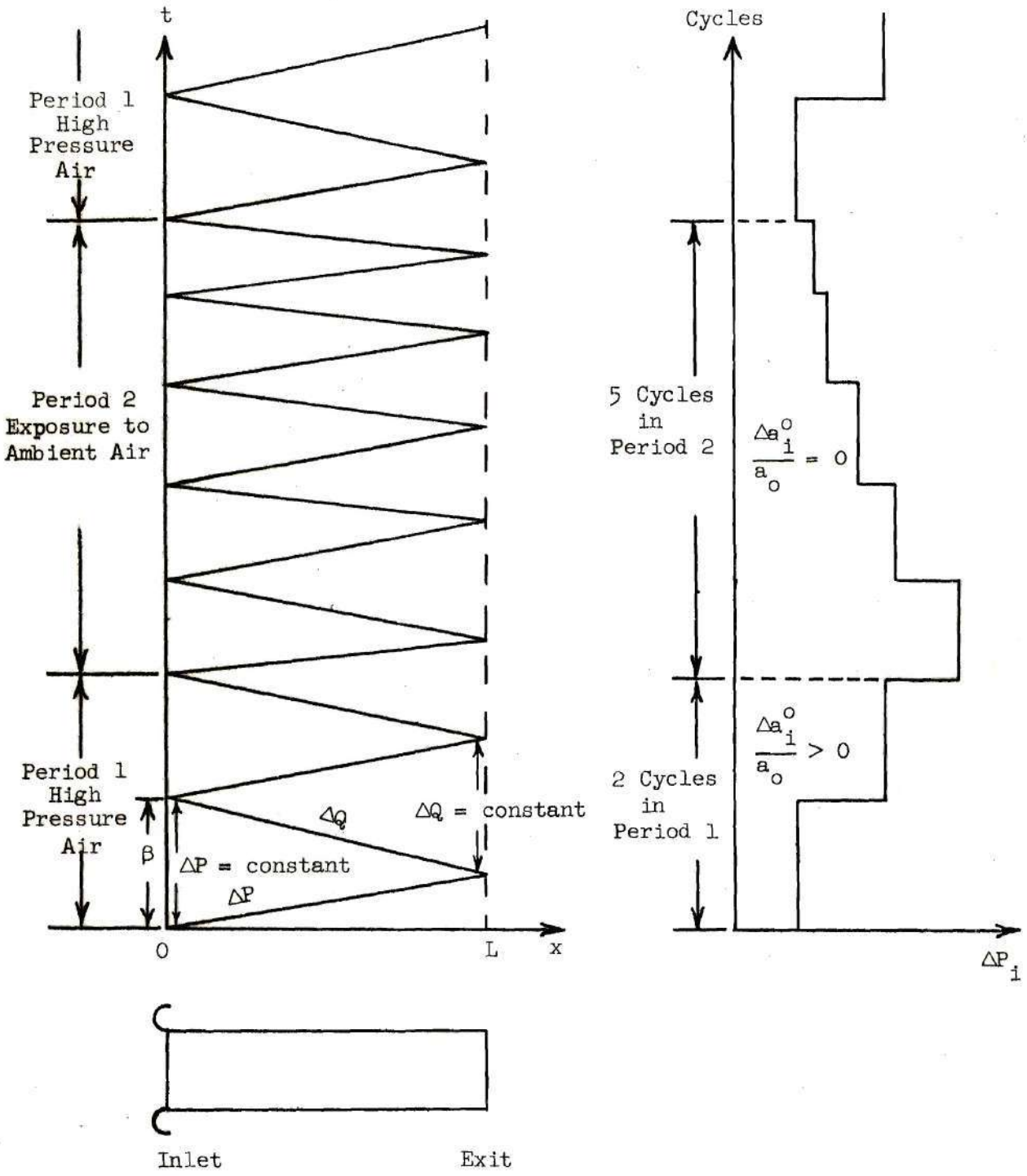

Figure 1. Wave Propagation and ΔP_{inlet} Change for Unsteady Flow in a Constant Area Duct. (Not to scale)

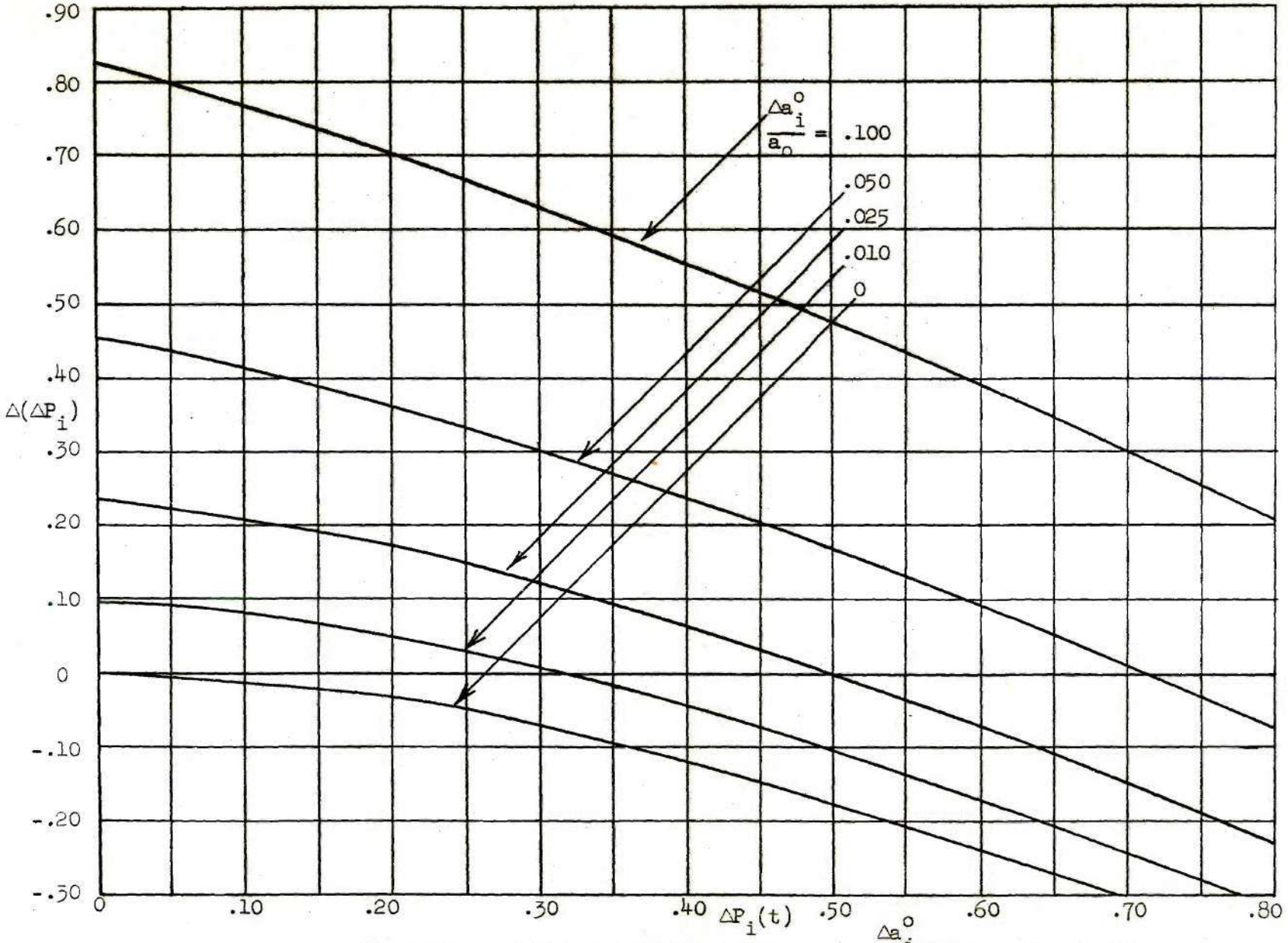

Figure 2. $\Delta(\Delta P_i)$ and $\Delta P_i(t)$ Relation for $\frac{\Delta a_i^o}{a_o}$ between 0 and .10.

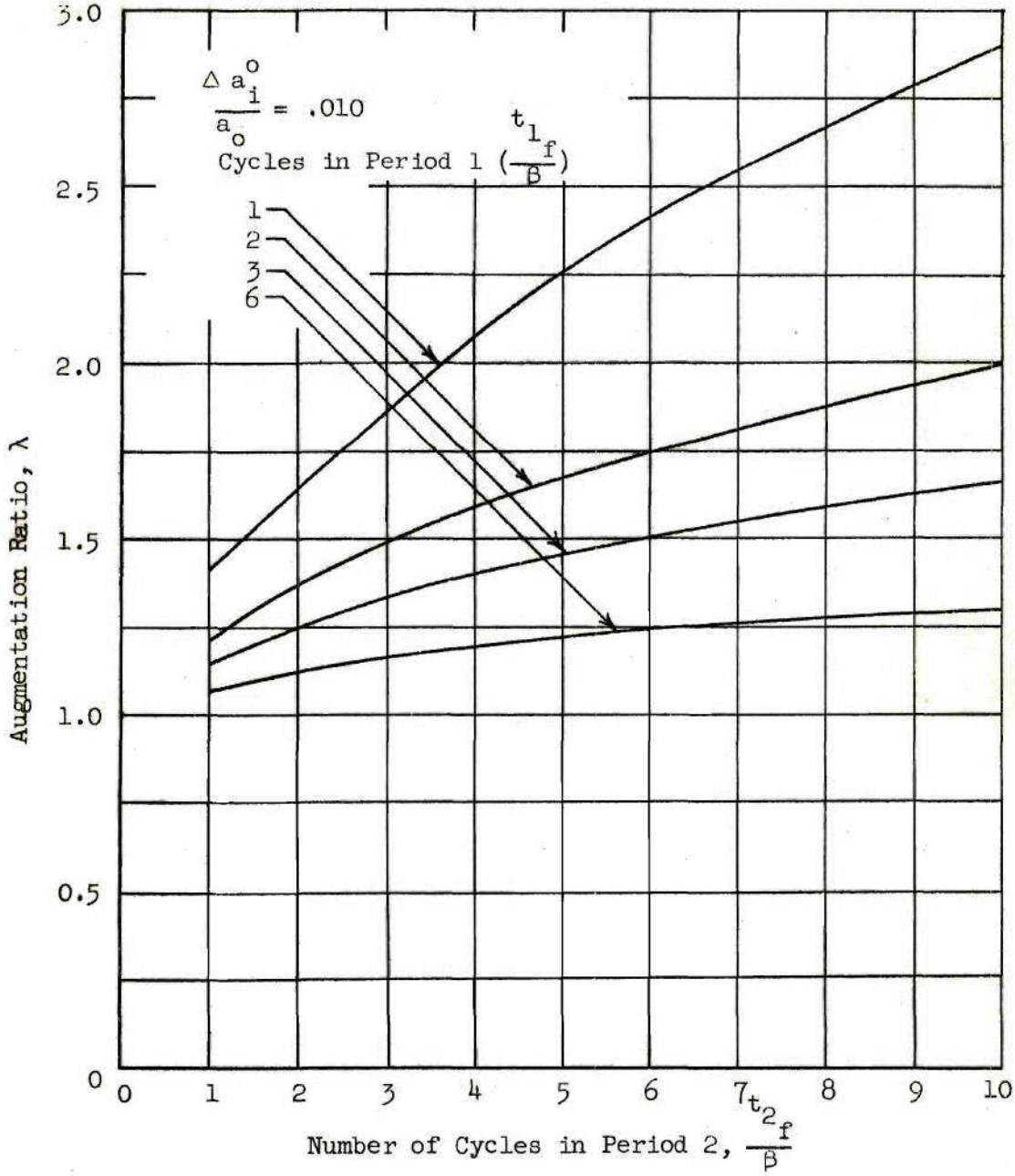

a. Effect of Number of Cycles in Period 2.

Figure 3. Effects of Independent Parameter Variation on Augmentation Ratio, λ. (Continued)

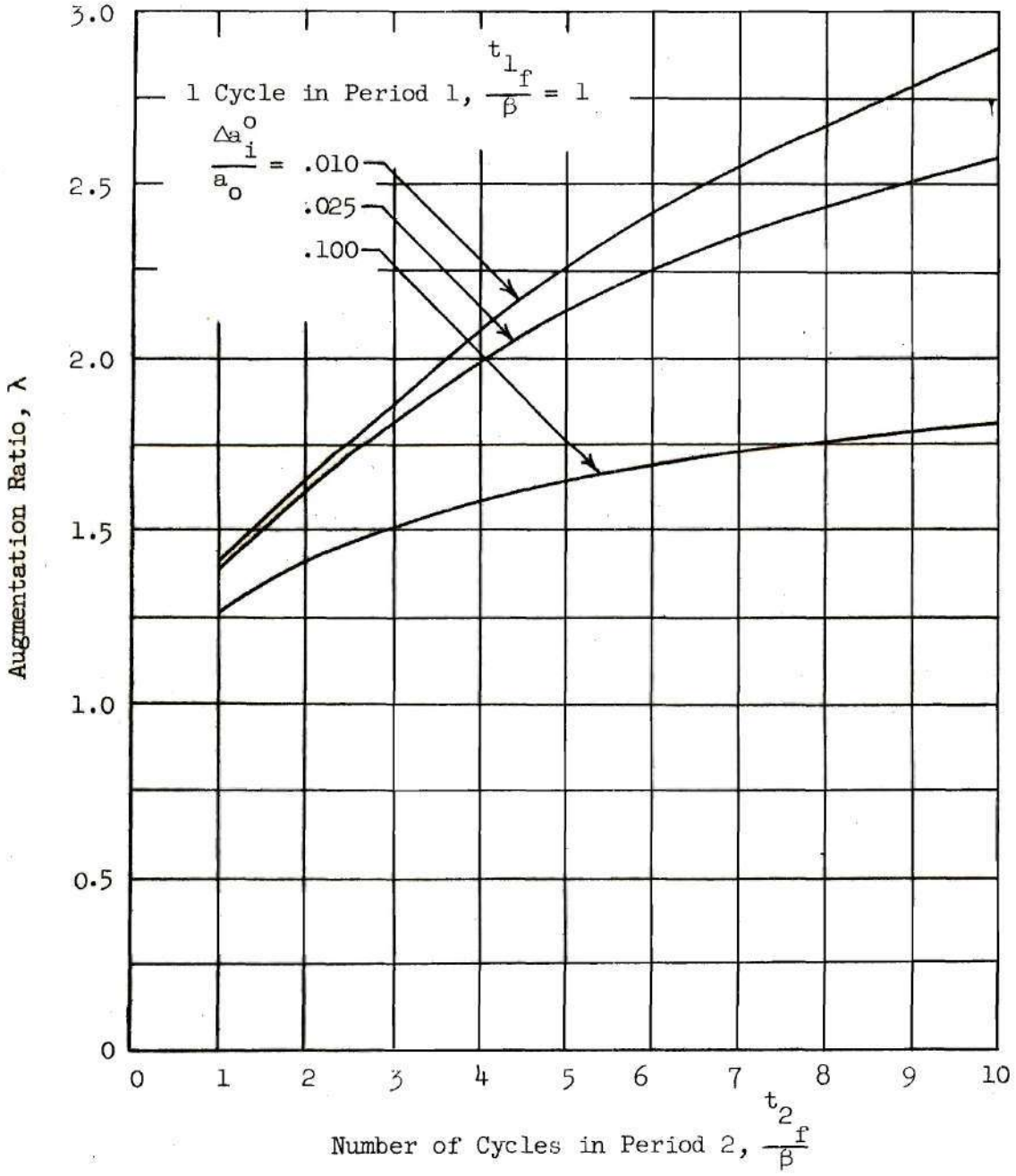

b. Effect of Pressure Ratio.

Figure 3. Effects of Independent Parameter Variation on Augmentation Ratio, λ.

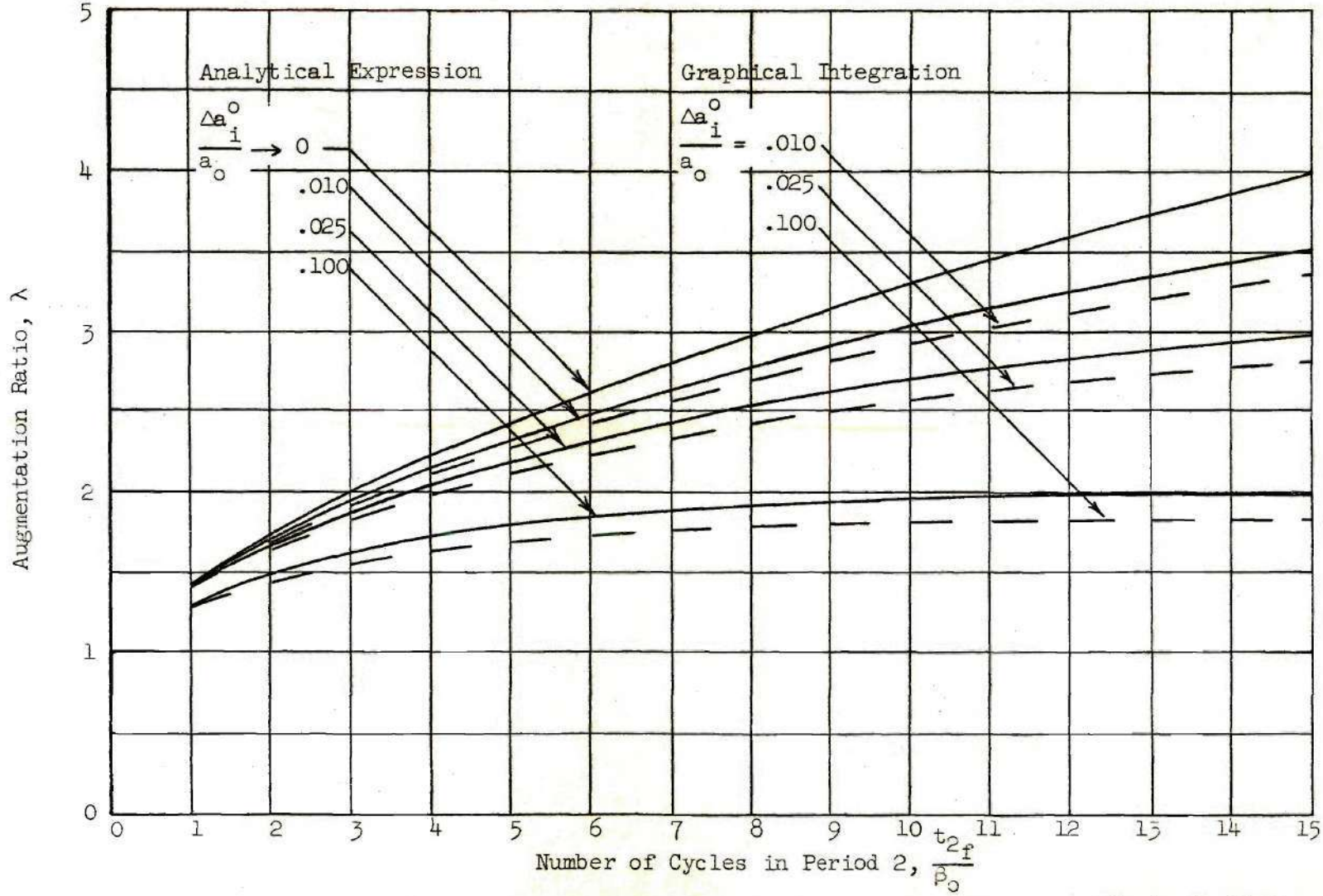

Figure 4. Comparison of Analytical and Graphical Solutions for Unsteady Flow Augmentation Ratio - One cycle in Period 1, $\frac{t_{1_f}}{\beta_o} = 1.$

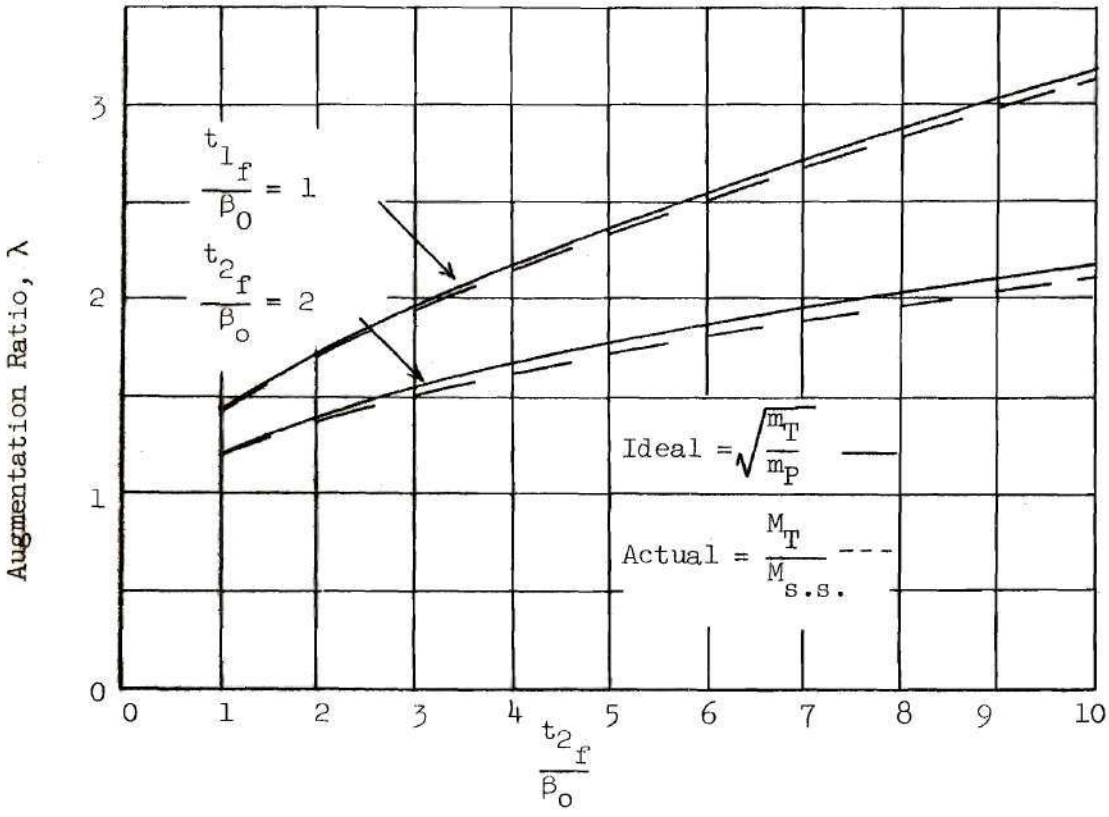

a. Direct Comparison of Ideal to Actual Augmentation Ratio Values.

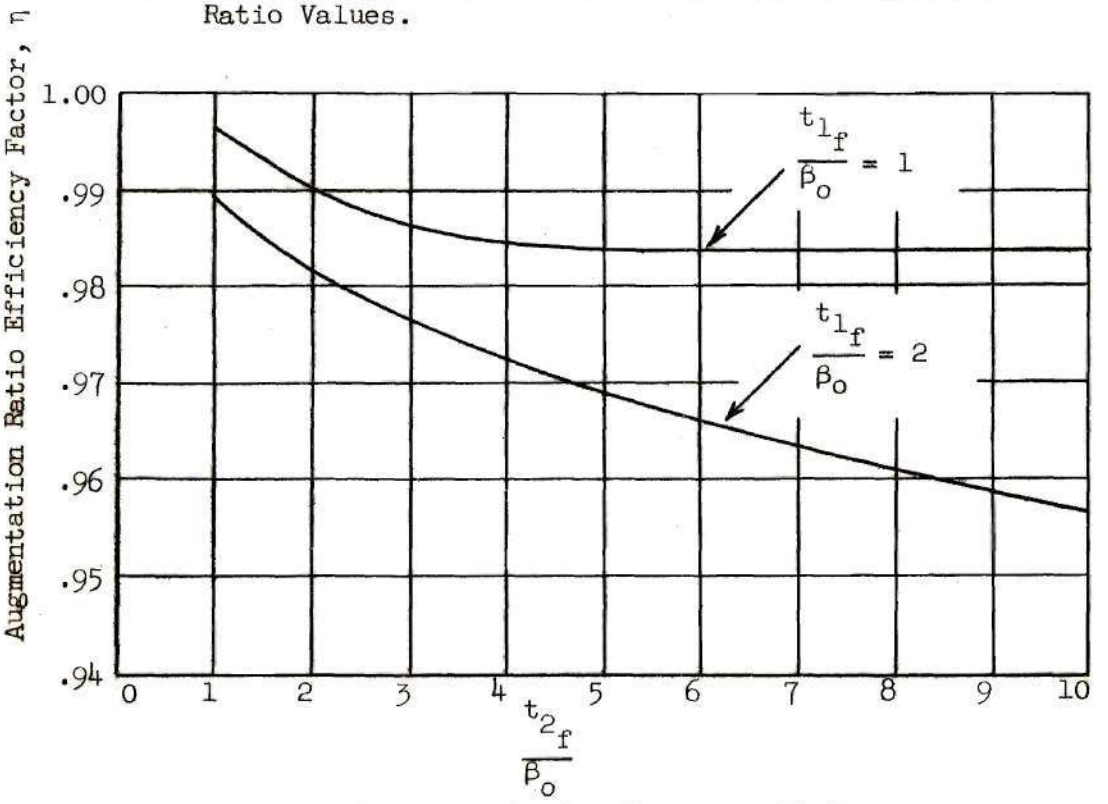

b. Augmentation Ratio Efficiency Factor.

Figure 5. Comparison of the Ideal to the Actual Augmentation Ratios, $\frac{\Delta a_i^o}{a_o} = .010$.

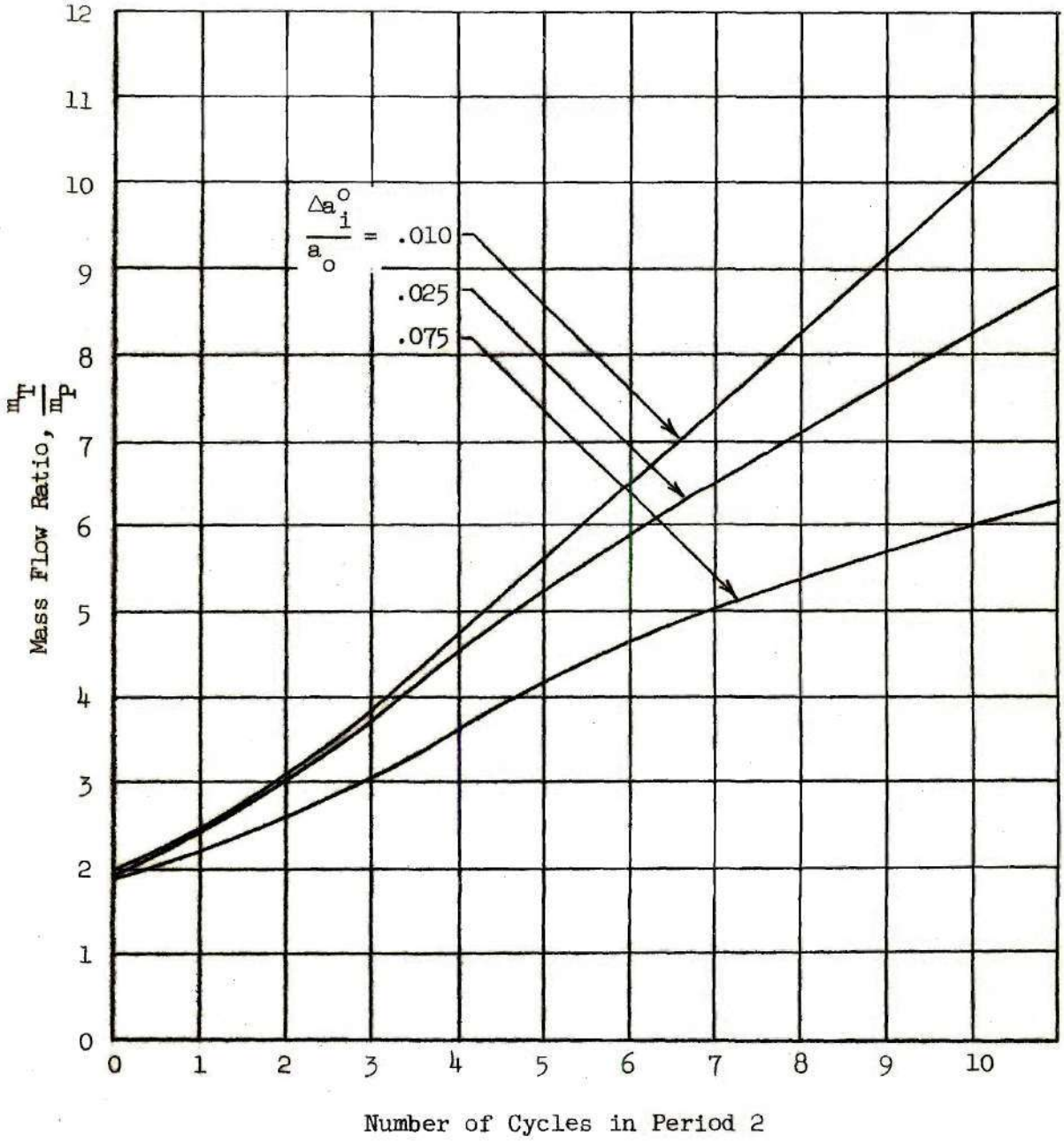

Figure 6. Effect of Pressure Ratio Variation on the Mass Flow Ratio. One Cycle in Period 1, $\frac{\tau_{1_f}}{\beta_o} = 1$.

Case 1.

Case 2.

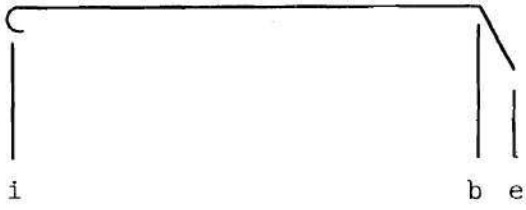

Figure 7. Extreme Cases of the Diverging Duct Analysis.

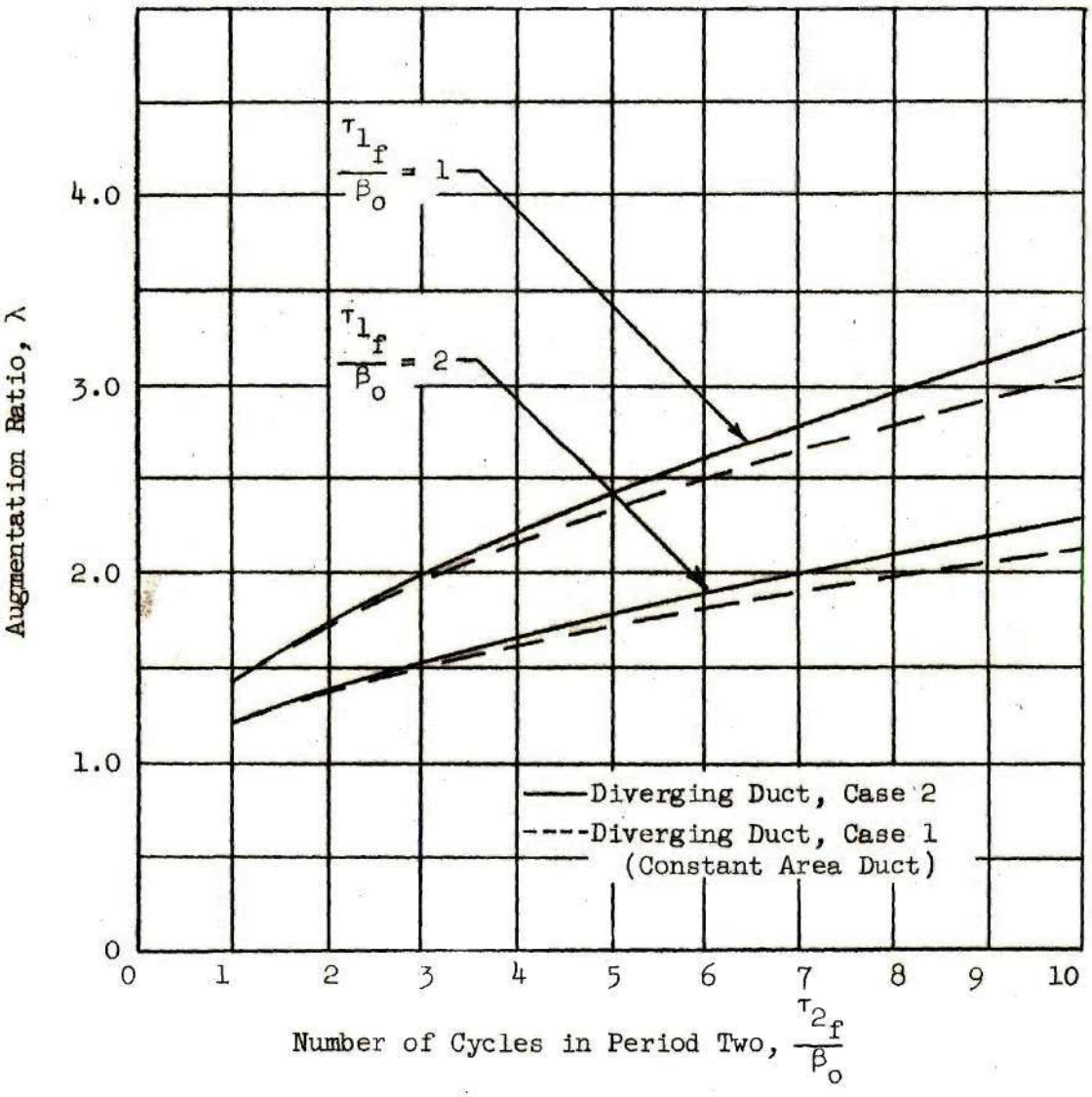

Figure 8. Augmentation Ratios for the Extreme Cases of the Diverging Duct, $\frac{\Delta a_i}{a_o} = 0.1$ for $\frac{\tau_{1_f}}{\beta_o} = 1$ and 2. $\frac{\alpha_i}{\alpha_e} = .5$.

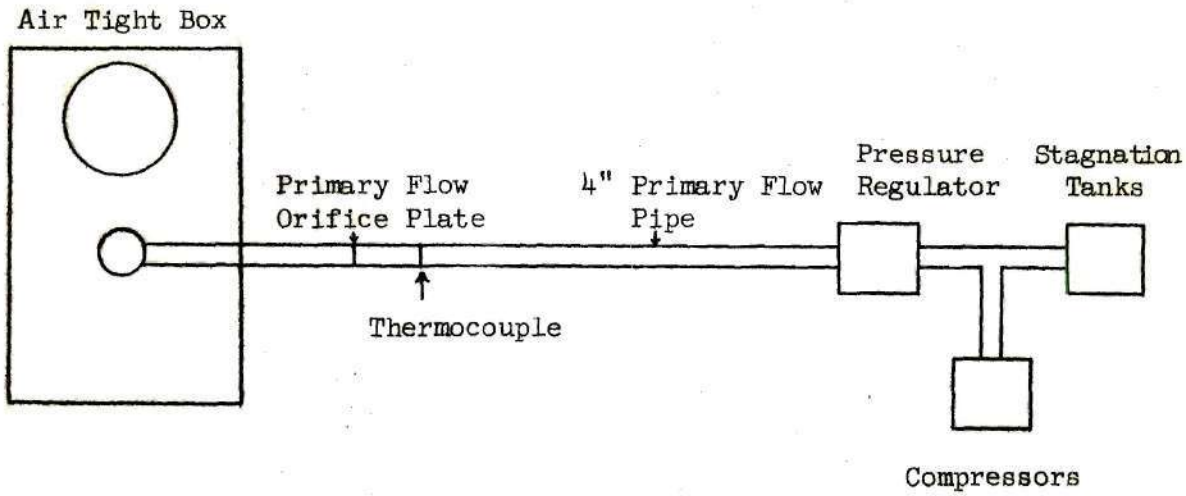

a. Side View

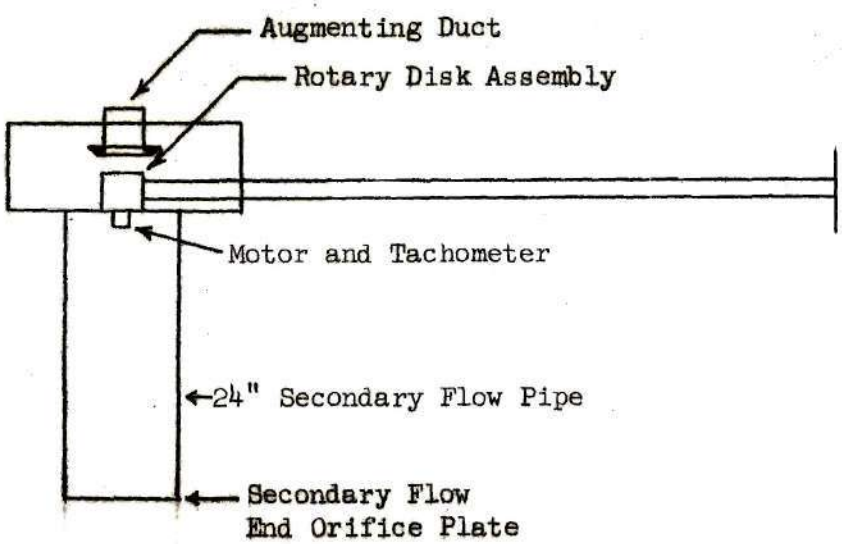

b. Top View

Figure 9. Test Apparatus Installation Schematic.

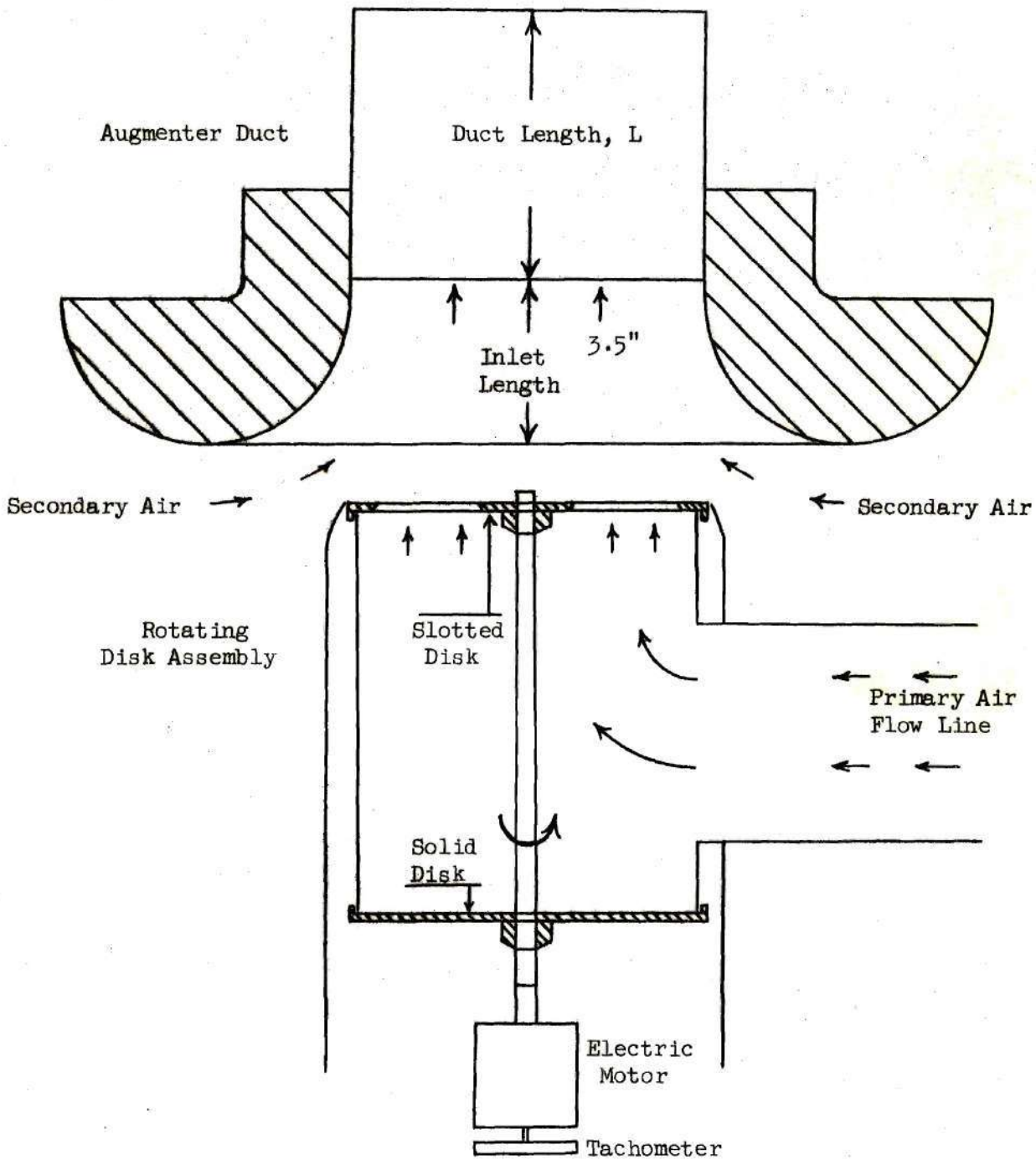

Figure 10. Cross Section of Augmenter Test Apparatus.
(Scale 1" = 3")

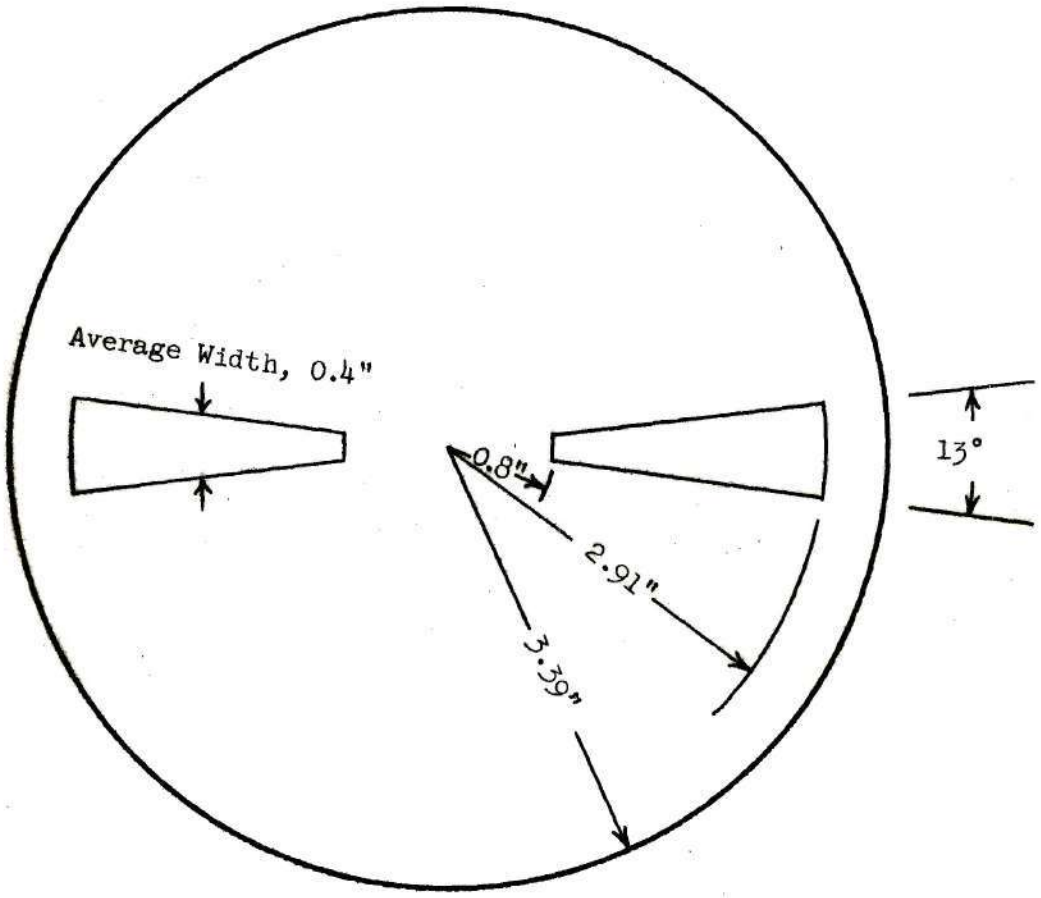

Figure 11. Augmenter Slotted Disk (Scale 1" : 1.5")

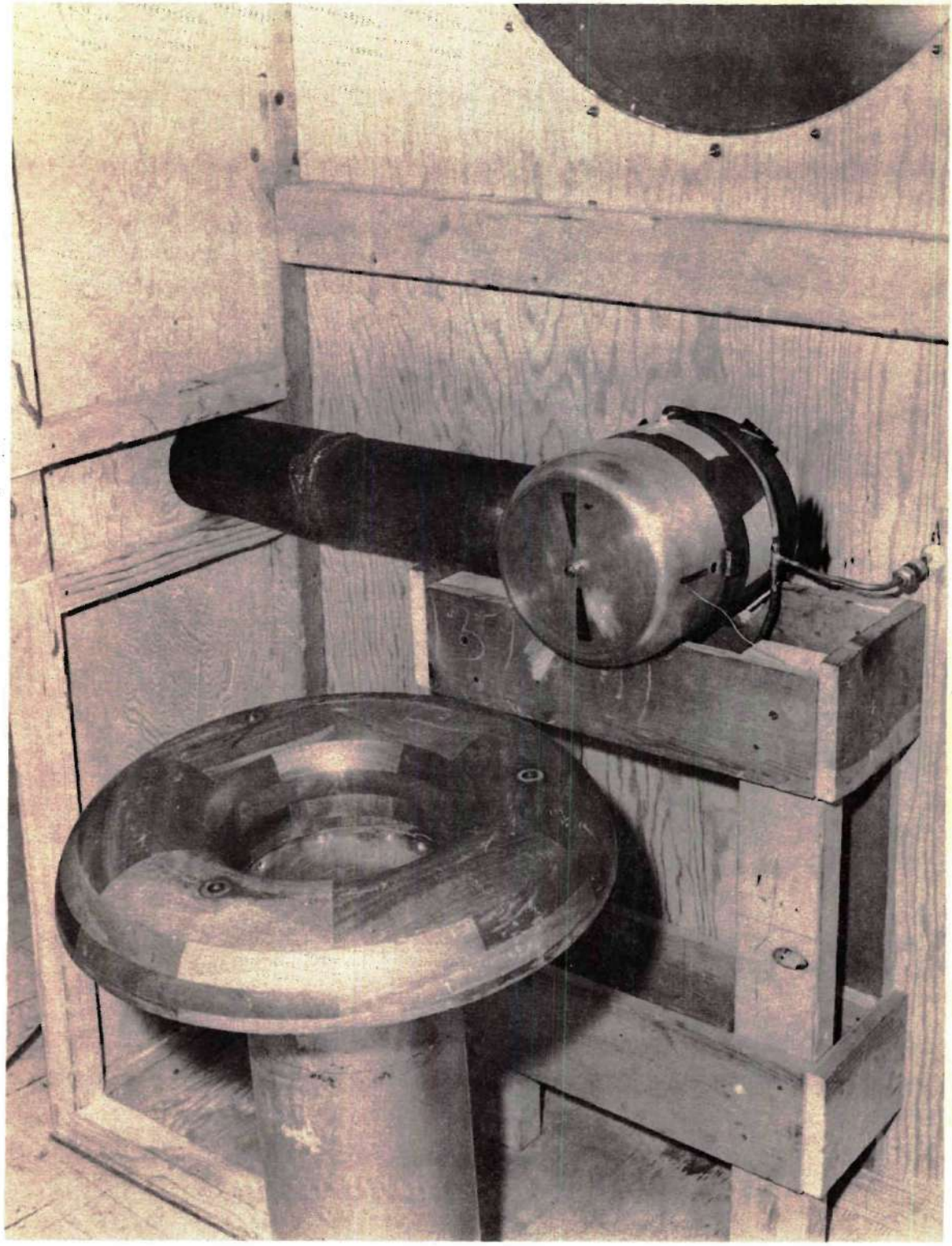

Figure 12. Photograph of Augmenter Test Apparatus.

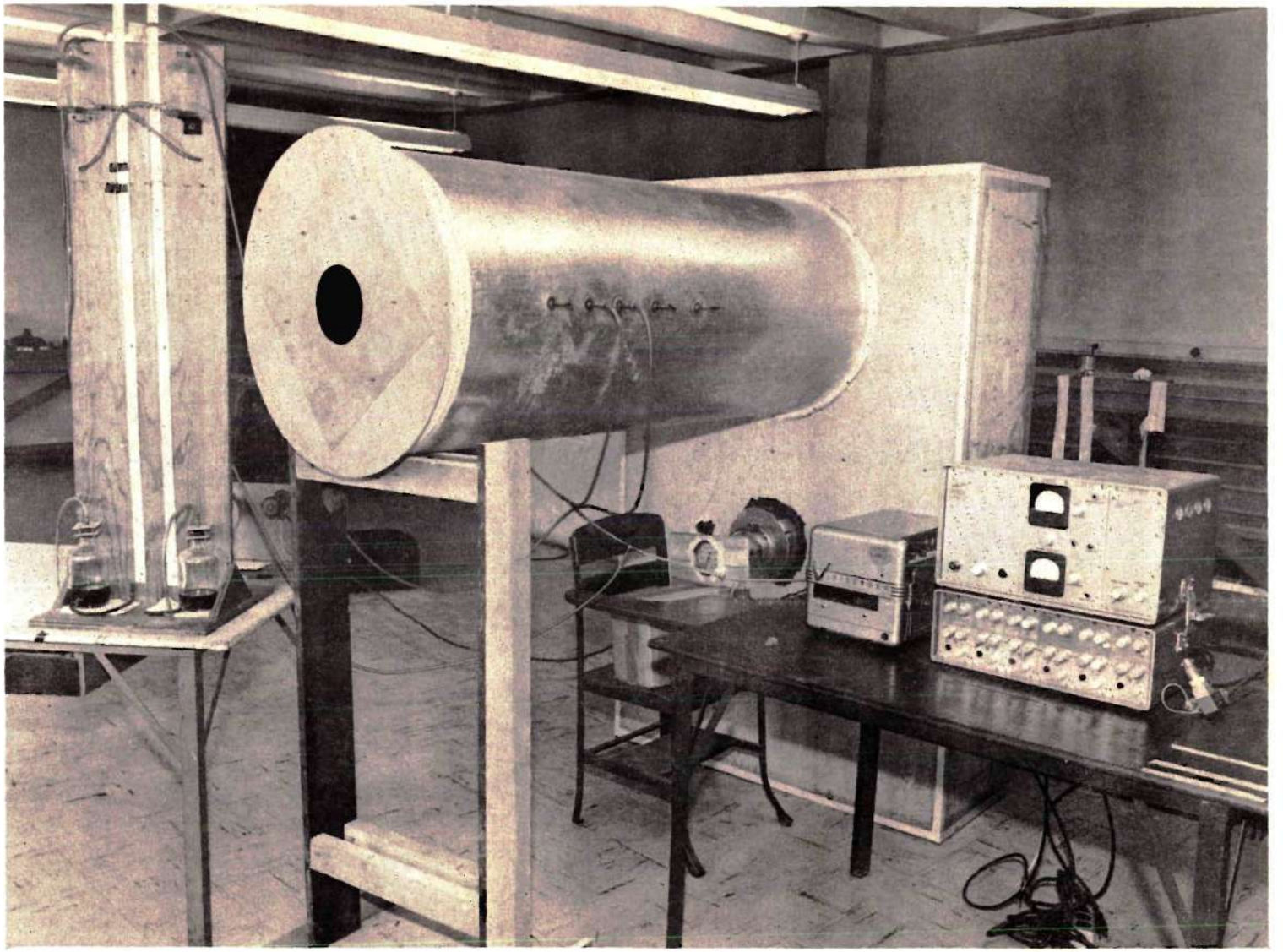

Figure 13. Photograph of Test Apparatus Installation and Instrumentation.

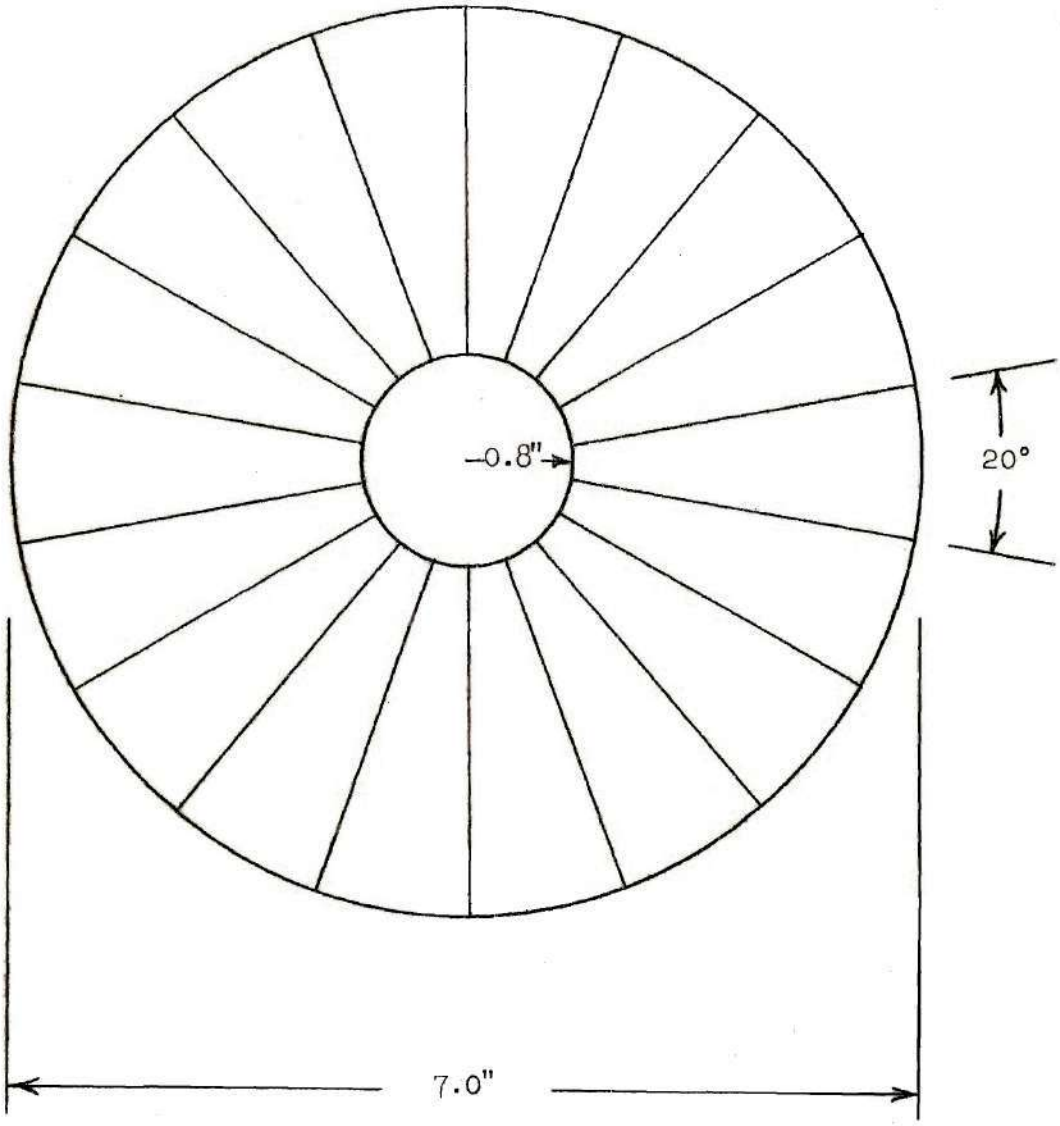

Figure 14. Cross Section of Augmenter Duct with Separator Vanes Installed.

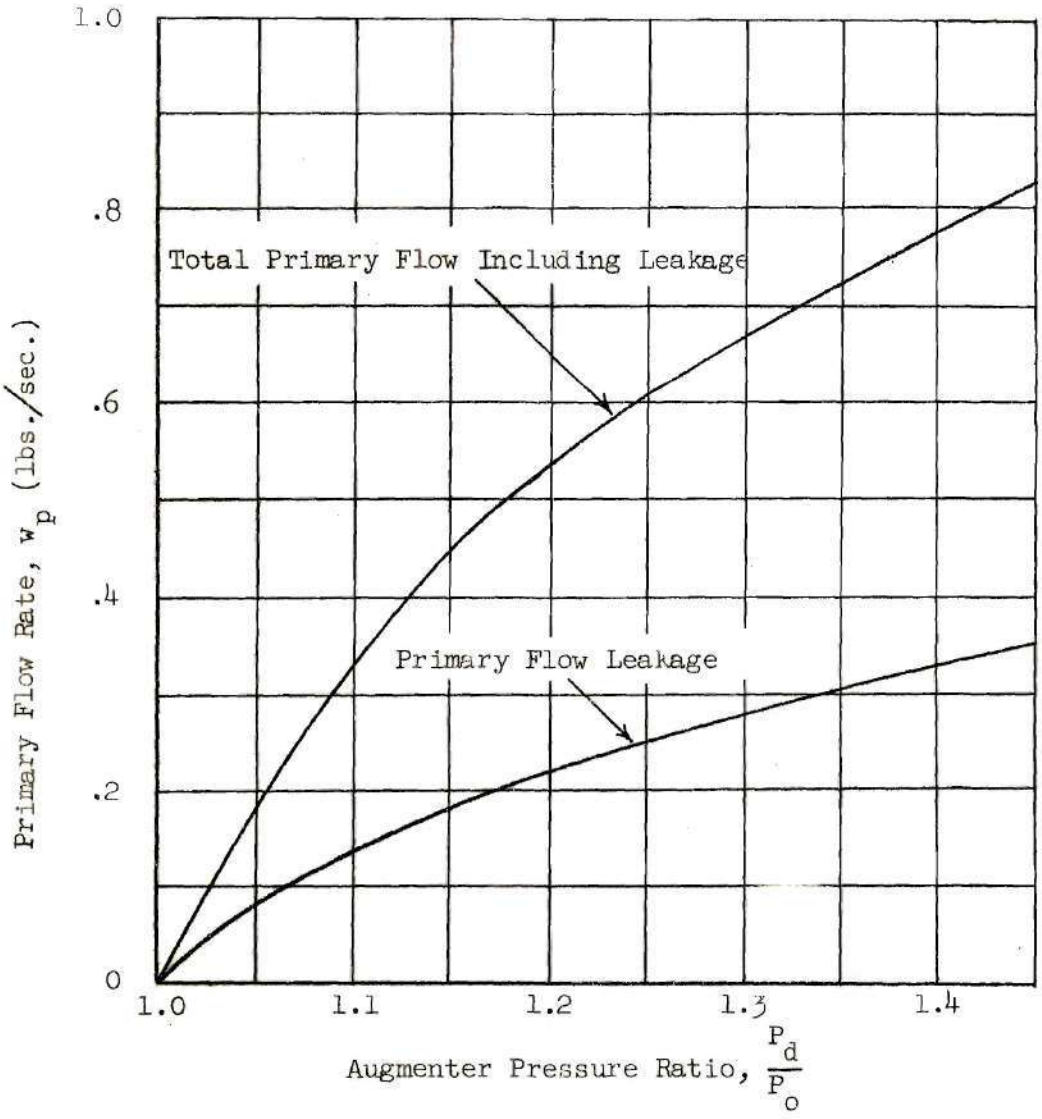

Figure 15. Test Apparatus Primary Flow Rate and Leakage.

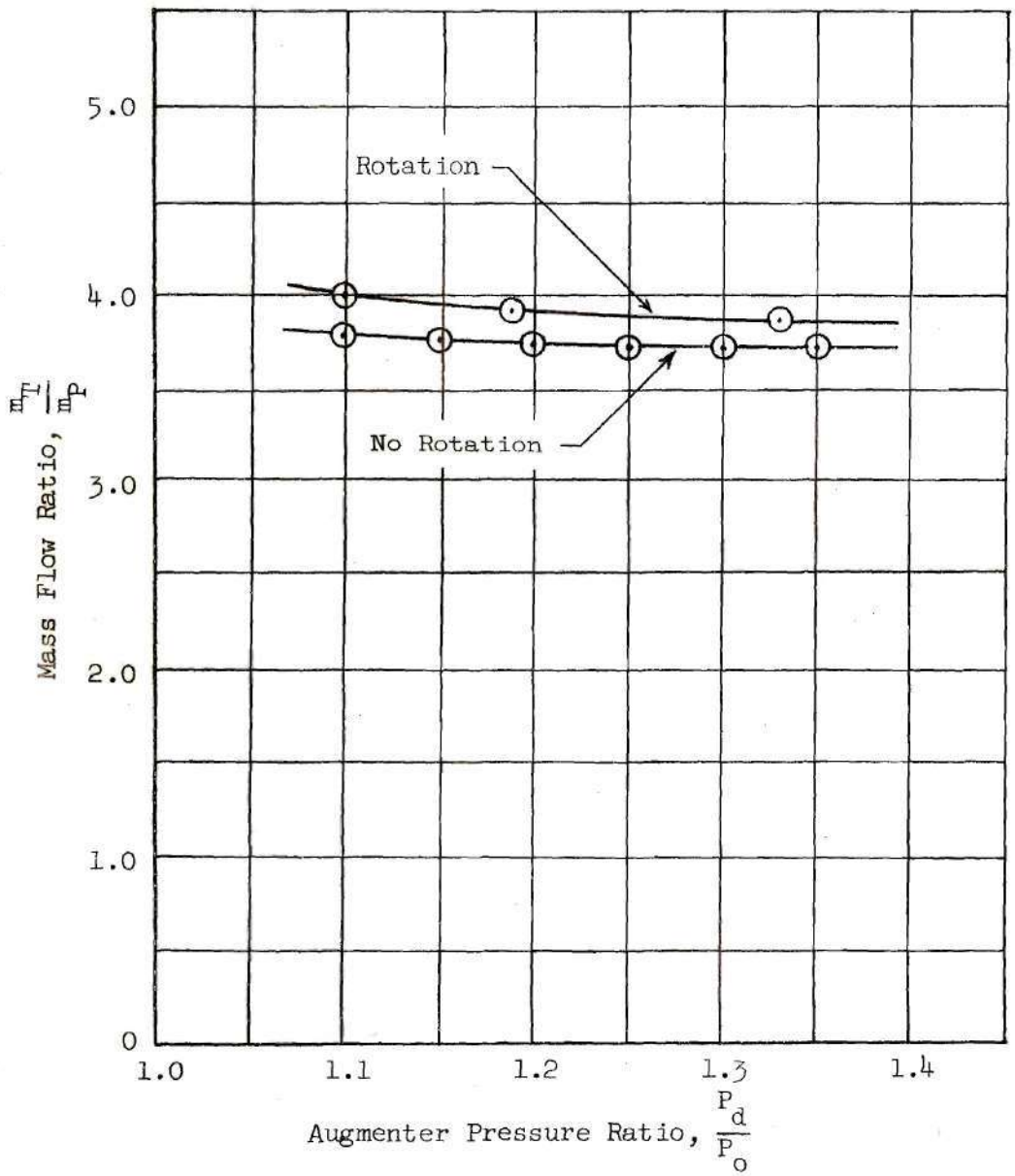

Figure 16. Experimental Augmenter Performance, 23" Duct Without Separator Vanes.

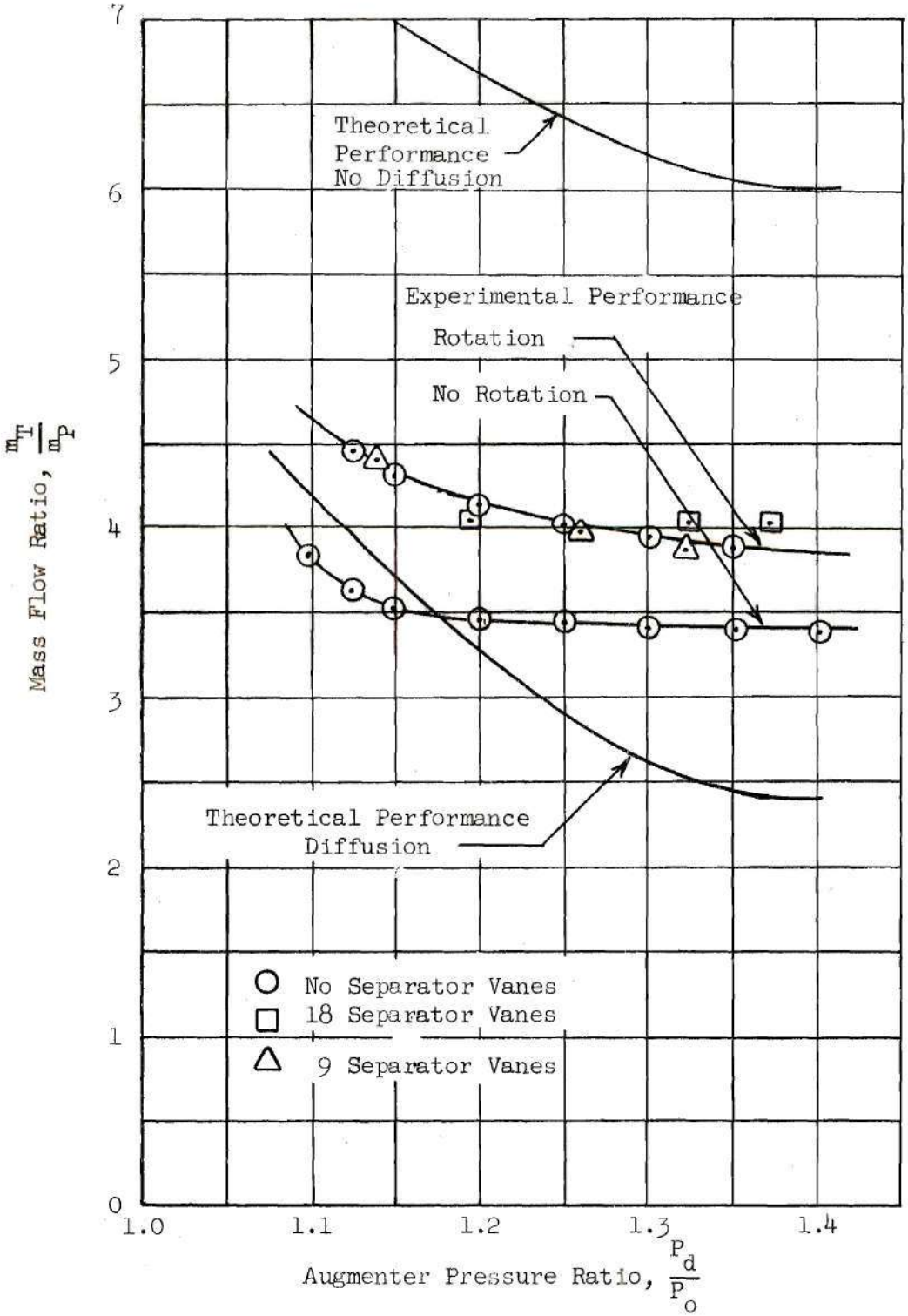

Figure 17. Experimental and Theoretical Augmenter Performance, 8.4" Duct With and Without Separator Vanes.

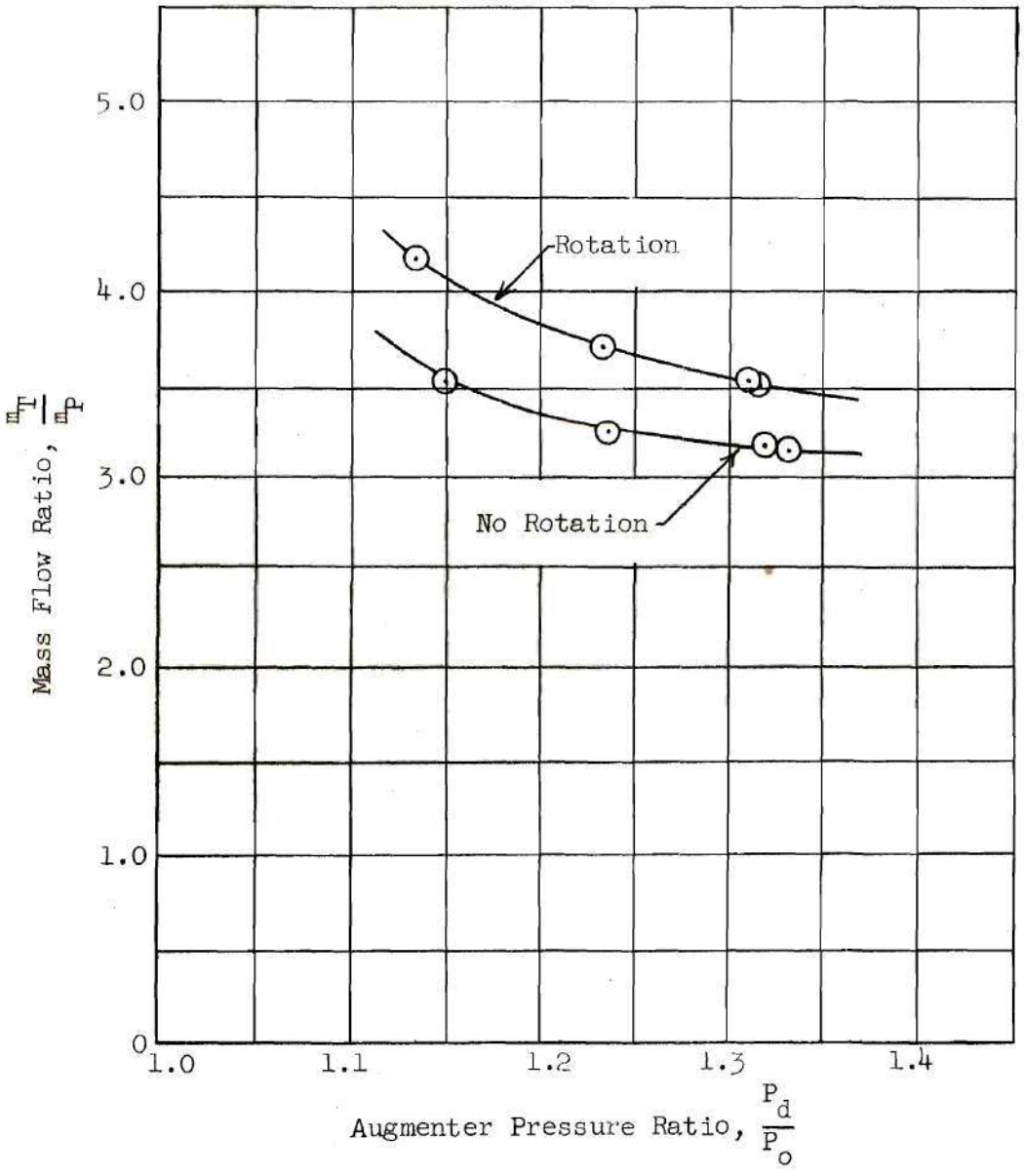

Figure 18. Experimental Augmenter Performance, 8.4" Duct and Modified Inlet Without Separator Vanes.

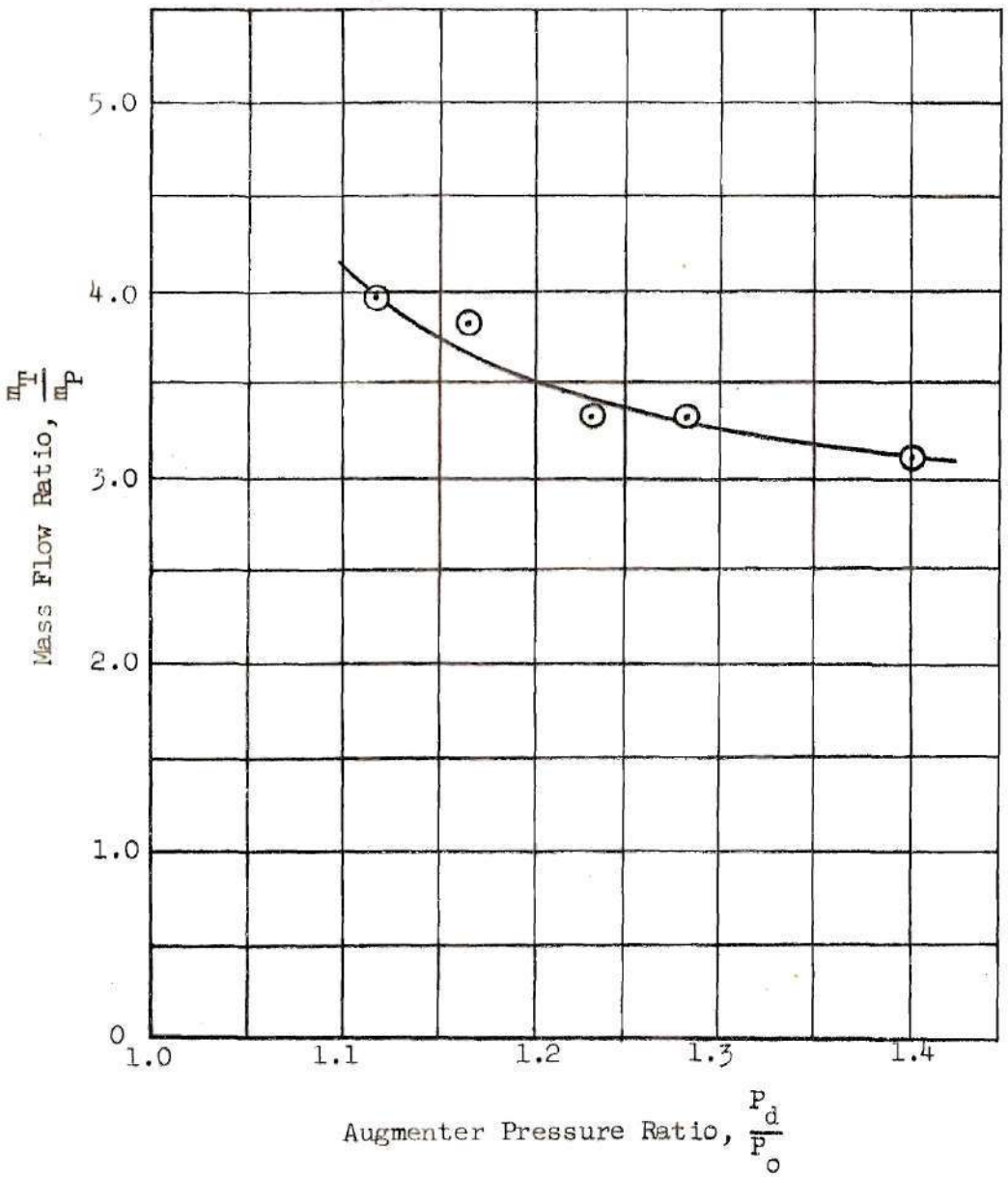

Figure 19. Augmenter Performance, 4" Duct and Modified Inlet with Separator Vanes.

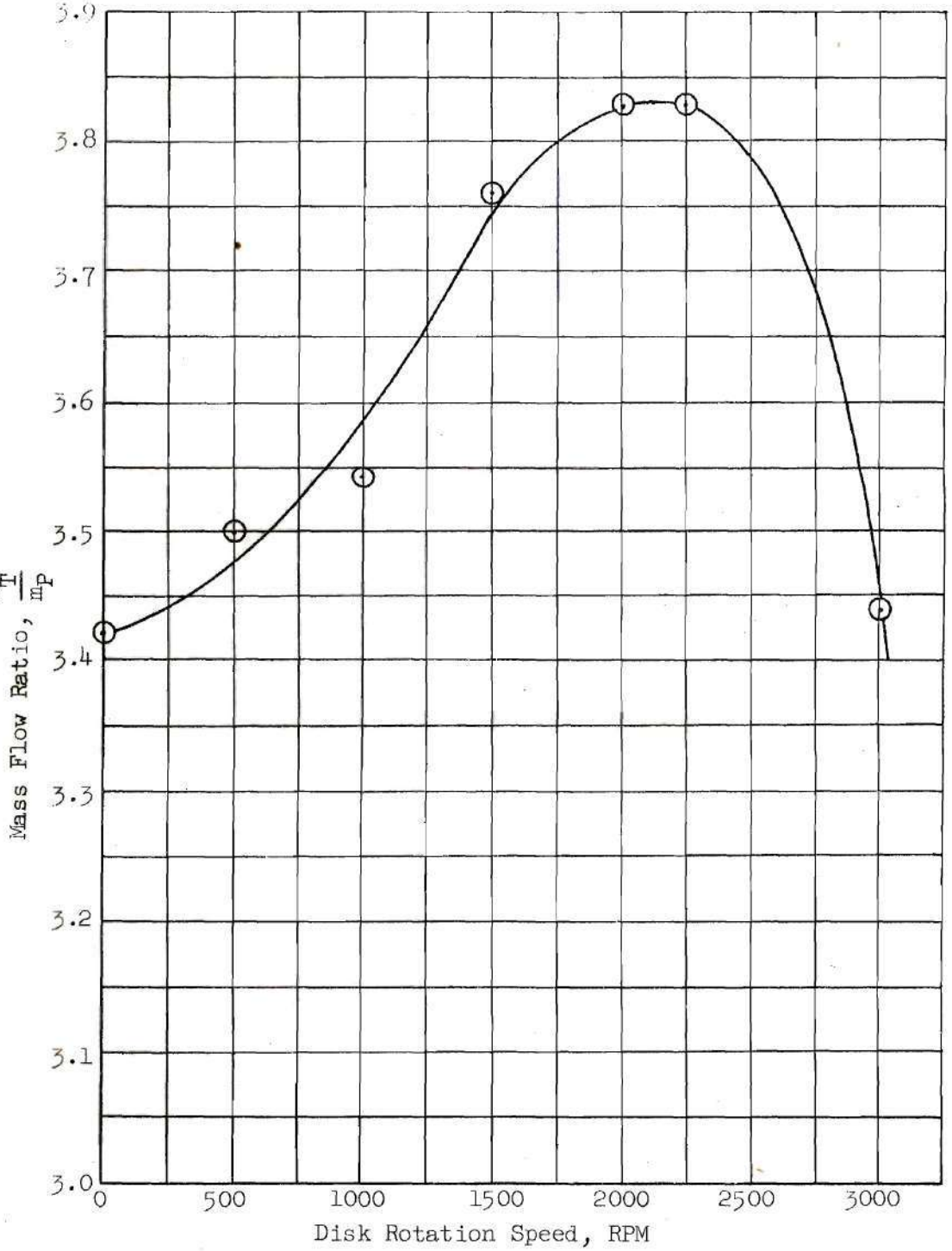

Figure 20. Pumping Ratio Variation with Disk Rotation Speed, $\frac{p_d}{p_o} = 1.3$, 8.4" Duct.

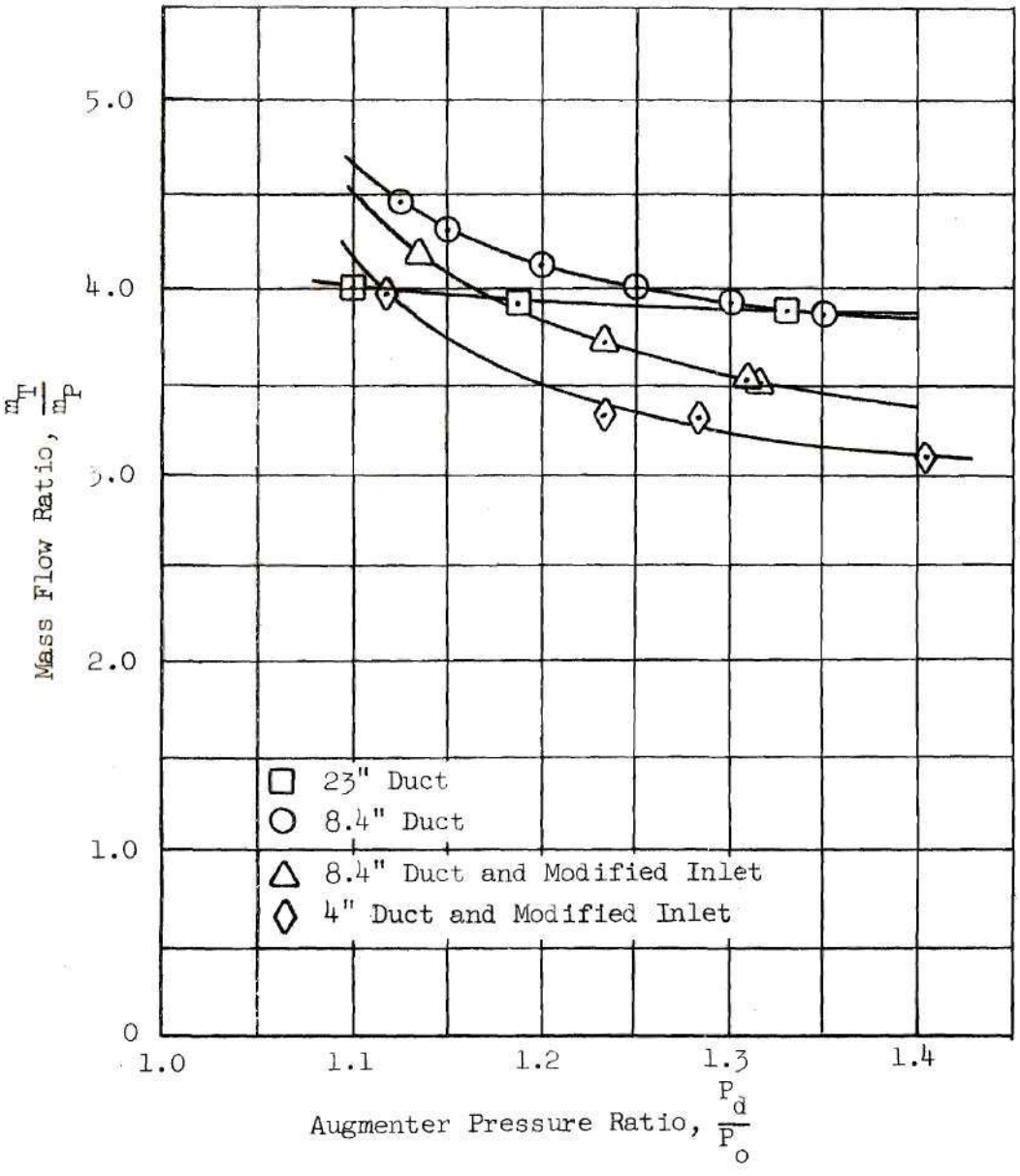

Figure 21. Comparison of Augmenter Performance for Duct Configurations Tested. (Disk in Rotation)

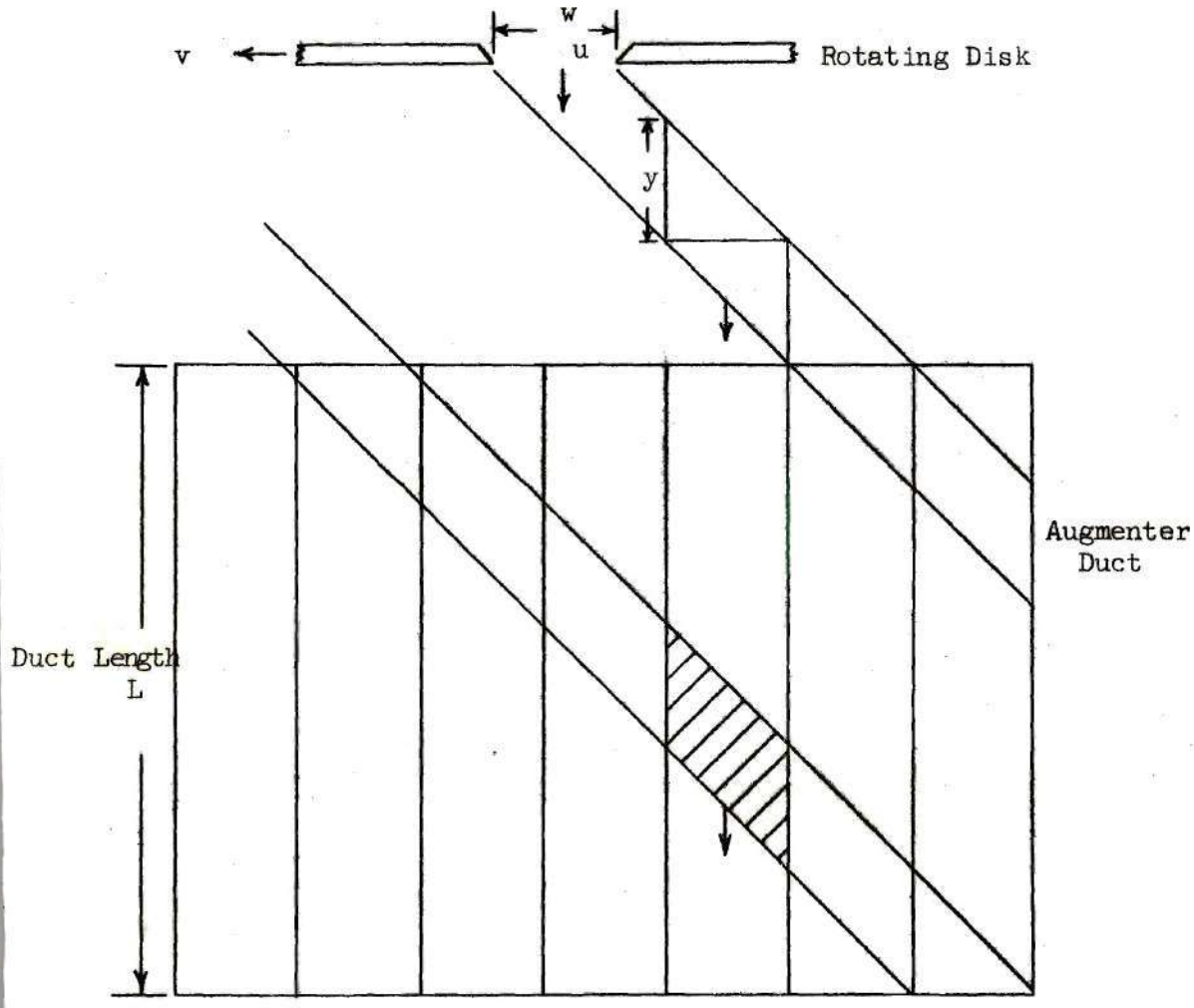

L = Duct length
u = Velocity of high pressure air through the disk slot
v = Average tangential velocity of the disk slot
w = Average width of the disk slot
y = High pressure air slug thickness

Figure 22. Cross Section of High Pressure Air Flow Pattern through the Slotted Disk and into the Augmenter Duct.

BIBLIOGRAPHY

1. Foa, J. V., Elements of Flight Propulsion, John Wiley and Sons, Inc., New York, 1960, pages 90-161.

2. Lockwood, R. M., "Interim Technical Report on Investigation of the Process of Energy Transfer from an Intermittent Jet to Secondary Fluid in an Ejector-Type Thrust Augmenter," Hiller Aircraft Corp., Report No. ARD-175, 30 September 1960.

3. Johnson, J. K., Shumpert, P. K., Sutton, J. F., "Final Report - Steady Flow Ejector Research Program," Lockheed - Georgia Company ER - 5332, September 1961.

4. Hohenemser, K. H., "Preliminary Analysis of a New Type of Thrust Augmenter," McDonnel Aircraft Corporation, presented at the Fourth U. S. National Congress of Applied Mechanics, University of California, Berkeley, California, 18-21 June 1962.

5. Foa, J. V., "Crypto Steady Pressure Exchange," Renssalaer Polytechnic Institute, TR-AE 6202, March 1962.

6. Shapiro, A. H., The Dynamics and Thermodynamics of Compressible Fluid Flow, Vol. II, Ronald Press Co., New York, 1954.

7. Rudinger, George, Wave Diagrams for Nonsteady Flow in Ducts, D. Van Nostrand Co., Inc., Princeton, N. J., 1955.

8. Stearns, R. F., Jackson, R. M., Johnson, R. R., Larson, C. A., Flow Measurement with Orifice Meters, D. Van Nostrand Company, Inc., New York, 1951.

9. Fluid Meters, Report of A.S.M.E. Special Research Committee on Fluid Meters, American Society of Mechanical Engineers, New York, 1937.